POLITECNICO
MILANO 1863

SCUOLA DI INGEGNERIA INDUSTRIALE
E DELL'INFORMAZIONE

Simulation and Testing of Navigation for an Autonomous Mobile Robot

Tesi di Laurea Magistrale in
Automation and Control Engineering - Ingegneria dell'Automazione

Author: **Giovanni Porcellato**

Student ID: 10745779
Advisor: Prof. Matteo Matteucci
Co-advisors: Simone Mentasti
Academic Year: 2021-22

Abstract

This thesis presents an integrated module for the simulation of a robot in a virtual environment, the creation of a testing platform and an attempt to solve the problems encountered during testing. The proposed approach thus offers both a solution to the complications encountered when testing hardware and a tool for collecting data and creating statistics in an automated manner.

The creation of the simulator benefits the development team, since they can take advantage of a system in which they can comfortably test new algorithms, without the risk of damaging the robot or its environment.

The creation of the testing platform serves the purpose of having solid data on which future performance improvements can be analytically evaluated.

Finally, the development of the image filter, responds to the need to solve problems related to certain light conditions that prevented the navigation stack from functioning correctly and consequently caused a degradation in performance.

Keywords: robotics, simulation, navigation, computer vision, image filter, testing platform

Abstract in lingua italiana

Questa tesi presenta un modulo integrato per la simulazione di un robot in ambiente virtuale, la creazione di una piattaforma testing e un tentativo di soluzione ai problemi riscontrati in fase di testing. L'approccio proposto offre quindi al contempo una soluzione alle complicanze che si incontrano quando si ha a che fa testing su hardware e uno strumento per raccogliere dati e creare statistiche in modo automatizzato.

La creazione del simulatore beneficia il team di sviluppo, dal momento che può sfruttare un sistema in cui testare comodamente i nuovi algoritmi, senza rischio di danneggiare il robot o l'ambiente circostante.

La creazione della piattaforma di testing risponde allo scopo di avere dei dati solidi su cui poter valutare i futuri miglioramenti delle performance in modo analitico.

Infine, lo sviluppo del filtro d'immagine, risponde all'esigenza di risolvere delle problematiche relative a certe condizioni di luce che impedivano il corretto funzionamento dello stack di navigazione e di conseguenza che causavano un degradamento delle performance.

Parole chiave: robotica mobile, simulatore, navigazione, visione computazionale, test

Contents

1 | Introduction

Now far from being science fiction, robots are little by little entering our world. The tendency to replace humans with machines has existed for centuries, but it is only during the 20th century that technology has enabled us to achieve astonishing results.
Hence, the robots we know today come in different forms: from robots with human form, to mechanical arms, to robotic heads. In each case, there was extensive research and development before arriving at the results we can enjoy today. Given the initial instability of robotic systems and the danger and cost, the creation of these devices went hand in hand with the development of special simulators.
It is indeed very inconvenient to repeat tests on hardware, for the reasons mentioned above. It is precisely in this circumstance that the need arises to simulate in a virtual environment the movements and actions that the robot would then have to repeat in the real world. It is therefore necessary to set up a testing procedure that has precise specifications and is reliable and repeatable over time.
In particular, the simulated behaviour of the robot must be consistent with the measurements and physical specifications of the robot in order to have a reliable simulation.
From an automation engineering point of view, the main objective is to eliminate human intervention even on the testing procedure, in order to have a semi-autonomous testing software, which returns data that can be easily analysed both for internal development and for supply to third parties.
The operator must in any case monitor the progress of the test in order to obtain useful information on anomalous behaviour. This work proposes a tool for testing the navigation of a humanoid robot in a simulated environment, offering a faithful and secure solution and obviating the problematic testing on hardware.
In addition, lateral solutions are presented to problems that arose in the testing phase, such as the denoising of the image received from the robot‘s video terminal.

1.1. Oversonic Robotics

This project has been realized as an application for Oversonic Robotics.
Oversonic Robotics is an Italian robotics start-up founded in 2020 in Besana in Brianza (MB) that wants to provide companies with intelligent systems that can assist humans in the most psychologically and physically demanding and exhausting jobs, thus enabling people to devote themselves to tasks that more effectively enhance intelligence. Their first project, Robee (Figure 1.1), is an autonomous humanoid robot, 1.75 m tall with a weight of around 75 Kg. He operationally replicates the mechanical structure of the human body, with 36 movable joints and a complete set of sensors. This enables him to see and navigate the surrounding space. The interaction is managed via a voice interface, capable of carrying out a normal conversation. He has arms and hands that allow him to cover all kinds of tasks. These include the simplest gestures such as pointing or counting, to a solid grip for handling objects. For greater awareness of his surroundings and for better communication with operators, Robee is equipped with a variety of cameras that use facial recognition and object detection.

Figure 1.1: "Robee", the humanoid robot developed by Oversonic Robotics Repubblica [20]

1.2. Contribution

The main contributions of this work are as follows:

- Development of a simulated environment to test the robot's new navigation features.
- Development of a module to test the navigation performance of the robot.
- Implementation of a point-cloud filter in order to improve obstacle handling and consequently navigation performance in critical brightness scenarios

1.3. Document Structure

The content is divided into two large sections: the first refers to the **Theoretical and Technological Background**, where the state of the art and the technologies used are introduced, in order to fully understand the system; the second one contains the **Contribution** of the thesis and reports the architecture of the system, its implementation and results. The thesis is composed of six chapters, below we list the content of each of them to give the reader an overview of the work done.

- Chapter 2 provides an overview of the software platform ROS, Robot Operating System, explaining its characteristic and philosophy that highlight why it is used as common platform to manage robots' operations, tasks, motions.
- Chapter 3 first introduces robots providing a brief historical overview. It is then described Oversonic robot, Robee, describing its components, both software and hardware.
- Chapter 4 aims to introduce the literature survey of the various techniques used for mobile robot navigation. Navigation and obstacle avoidance are one of the fundamental problems in mobile robotics, here are described two type of control global path planning and local motion control.
- Chapter 5 represents the main work of this thesis. It introduces first Gazebo simulator, afterwards it goes step by step through the building of the sim. robot and environment. It then encompasses the measurement module implemented. Results and issues are presented.
- Chapter 6 introduces point-cloud. This section proposes to solve an issue encountered while testing on the physical robot.

Theoretical background

From now on some basic knowledge needed to comprehend the reasoning of this work's study object is described and explained. This section consists of:

- **Chapter 2:** ROS
- **Chapter 3:** Robot
- **Chapter 4:** Navigation Stack

2 | ROS

2.1. Introduction

Platforms are becoming more and more significant in robotics. The two sorts of platforms are software platforms and hardware platforms. Low-level device control, SLAM (Simultaneous Localization and Mapping), navigation, manipulation, object or person recognition, sensing and package management, debugging and development tools are just a few of the characteristics that make up robot software platforms. These features are mostly used in the industrial sector, where robot software platforms are currently used most frequently. Robot hardware platforms include both industrial products and research platforms including humanoids, drones, and mobile robots. As a result, robotics researchers from around the world are working together to develop an open-source, user-friendly platform. Robot Operating System, sometimes known as ROS, is the most widely used robot software platform. The Robot Operating System, or ROS, is an open source framework for controlling the actions, motions, and other aspects of robots. In addition to those who have just started using robots, ROS is designed to be a software platform for both those who regularly develop and use robots.

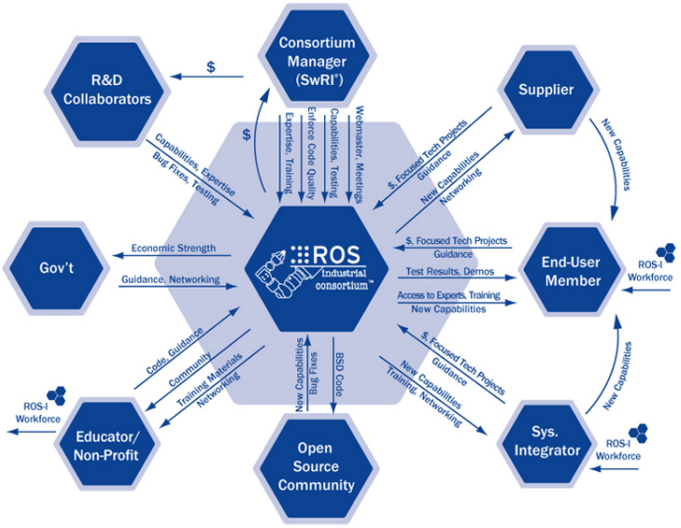

Figure 2.1: ROS Industrial Consortium

2.2. History of ROS

In the 1970s, the first specialized programming languages for robots emerged. Robot-specific data types and libraries of robot functions existed. They did not permit integrated simulation, multi-robot interaction, or hardware abstraction. Standardization and code reuse were nonexistent. Through the 1980s, 1990s, and particularly in the 2000s, when there was a strong drive to standardize robot components, their interfaces, and their fundamental functions, efforts to develop robot programming systems persisted.
ROS was therefore first created in 2007 at the Stanford Artificial Intelligence Laboratory, where it is still used today. It has been controlled by OSRF since 2013, and it is now utilized by numerous robots, academic institutions, and businesses, becoming the de facto norm for robot programming.

2.3. Meta-Operating System

ROS is merely a middleware because it is an open source, robot-specific operating system. A middleware is a piece of software that acts as a layer between the operating system and the applications, providing the developer with an additional degree of abstraction. It simply acts as a mediator between software parts, allowing for easier communication. Its function is to give an abstraction model for functions and the low-level implementation at the same time. Each middleware product must offer:

- Portability: common programming model regardless the programming language and system architecture
- Complexity management: low-level aspects are managed by libraries and drivers inside the middleware itslef
- Reliability: middleware allows robot developer to discard low level details
- Abstraction from sensors/actuators hardware;
- Communication protocol for data transport

As a result, they are crucial to the creation of sophisticated programs that rely on a variety of hardware and software resources.
They still need to go through a lot of development before they can offer a full range of capabilities for general-purpose robots.

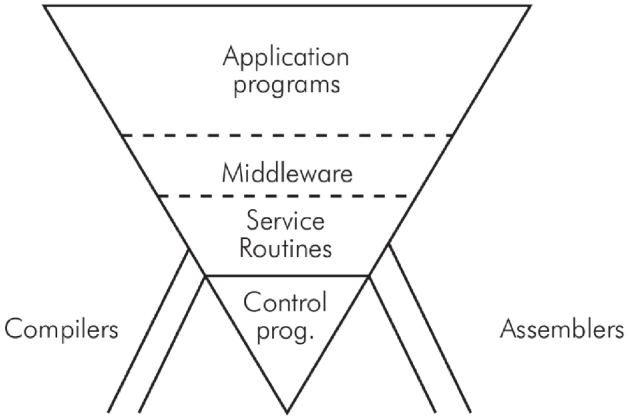

Figure 2.2: Meta Operating System

In recent years, a number of robotic middlewares (OROCOS, ORCA, YARP, BRICS, etc.) were put forth; eventually, ROS emerged.

2.3.1. Phylosophy of ROS

Some philosophical facets of ROS are described in the following sentences:

- *Peer to peer*: ROS systems are composed of a small number of interconnected computer applications that are continuously exchanging messages. These communications flow directly between programs. The system becomes more complex as a result, but as the amount of data grows, the system balances better.

- *Distributed*: Programs can be run on multiple computers and comunicate over the network.
- *Multilingual*: ROS decided on a multilingual strategy. Any language that has a client library created for it can be used to create ROS software modules. Client libraries are available for C++, Python, LISP, Java, JavaScript, MATLAB, and other programming languages as of this writing.

- *Thin*: contributors are encouraged to build standalone libraries by the ROS conventions. and then wrap those libraries, so that they can send and receive messages to and from other ROS modules. This additional layer is proposed to allow the reuse

of software developed outside of ROS for other applications, and it greatly simplifies the development of automated tests using standard continuous integration tools..

- *Free and open source*: Free and open source: The permissive BSD license is used to release the ROS core, which allows both commercial and non-commercial use. ROS foresees data exchange between modules using inter-process communication (IPC), which means that systems built using ROS can have fine-grained licensing of their various components.

2.4. ROS Architecture

Based on a graph architecture, ROS allows for processing to occur in nodes, which exchange messages with one another synchronously by calling services, much like RPCs, and asynchronously by using topics to which they can subscribe and/or publish. In terms of structure, ROS is created on three conceptual levels:

1. File-system level
2. Computational level
3. Community level

We'll look at each level's individual components and how they fit into the architecture.

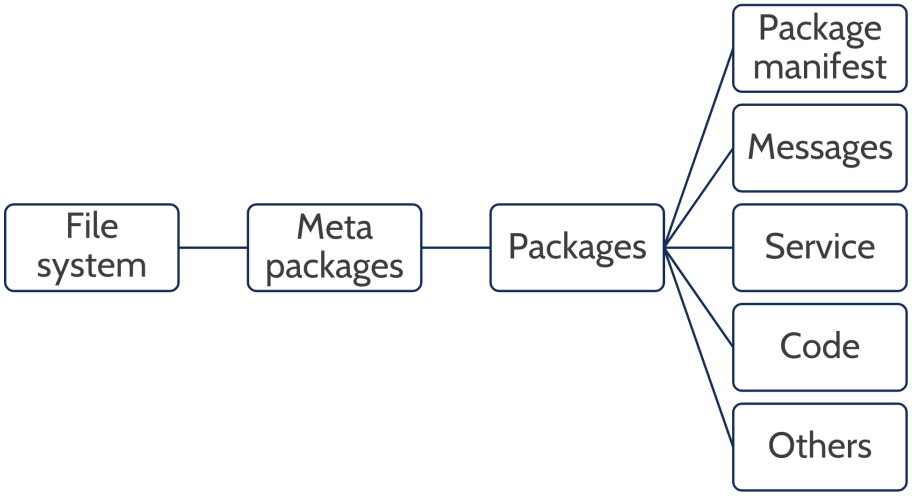

Figure 2.3: File System level representation

2.4.1. File-system Level

The Filesystem Level includes all resources used in ROS, in particular

- Packages
- Metapackages
- Manifest
- Message types
- Service types

Packages
Packages are the main structure for organising ROS, Wiki [32]. These files include all of the data needed by the system during runtime, including processes, libraries, configuration files, datasets, and other files. They make up the structural elements of a ROS-based system. The package is represented by a directory at the filesystem level.

There are some subfolders within the framework to manage the elements in order to encourage its growth:

- *include/packagename*: C++ include headers (make sure to export in the CMakeLists.txt)
- *msg*:Folder containing Message (msg) types
- *src/packagename*: Source files, especially Python source that are exported to other packages.
- *srv/*: Folder containing Service (srv) types
- *scripts*: executable scripts
- *CMakeLists.txt*: CMake build file
- *package.xml*:XML file containing package structure
- *CHANGELOG.rst*: Many packages will define a changelog which can be automatically injected into binary packaging and into the wiki page for the package

Metapackages Metapackages are specialised structures whose only task is to represent a group of packages that have common characteristics with each other. The metapackages that are created in the context of older versions of ROS and later updated may also result from the conversion of older stacks that perform similar functions in the context of older versions of ROS, Wiki [29].

Manifest

A package manifest consists of an XML file named package.xml that must be included in the root folder of any catkin-compliant package. It contains information about the package, including its name, version number, authors, maintainers, and dependencies on other catkin packages. There is a strong similarity between this concept and the manifest.xml file used in the legacy rosbuild build system. System package dependencies are declared in package.xml, Wiki [28].
There are a minimal set of tags that need to be nested within the <package> tag to make the package manifest complete.

- *<name>*: The name of the package
- *<version>*: The version number of the package;
- *<description>*: A description of the package contents;
- *<maintainer>*: The name of the person(s) that is/are maintaining the package;
- *<license*: The software license under which the code is released.

Message types

Message types define the structure of messages sent by ROS, Wiki [30]. A separate sort of message is represented by each file with the.msg extension. Each line in the file corresponds to a message field. Each line has two columns: one for the field's data type (Int32/int (C++/Phyton), bool, string, time, etc.), and the other for the field name. The fields contained within these le can have values assigned to them; in this case, we're talking about constants. Msg file example in C++:

Service types

Service type are files that define the structure of request/response for ROS services, Wiki [35]. These directly build on the msg format to allow node-to-node communication. They are kept in specialized.srv files in a package's srv/ subdirectory. Srv file example in C++:

```
bool add(beginner_tutorials::AddTwoInts::Request  &req,
         beginner_tutorials::AddTwoInts::Response &res)
  {
    res.sum = req.a + req.b;
    ROS_INFO("request: x=%ld, y=%ld", (long int)req.a, (long int)req.b);
    ROS_INFO("sending back response: [%ld]", (long int)res.sum);
   return true;
 }
```

2.4.2. ROS Computational Graph Level

The peer-to-peer network of ROS processes that are working together to process data is known as the Computation Graph. Nodes, Master, Parameter Server, messages, services, topics, and bags are the fundamental Computation Graph concepts of ROS. Each of these components provides data to the Graph in a different manner, Wiki [27].

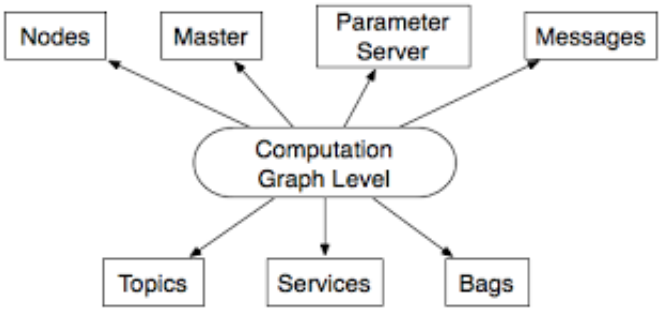

Figure 2.4: Computation Graph

Nodes

A node is a process that performs computation. Nodes are combined together into a graph and communicate with one another using streaming topics, RPC services, and the Parameter Server, Wiki [31]. In accordance with the concept of modularity of the system, each node will be connected to just one specific functionality. In order to make the system more reusable, manageable, and understandable, ROS actually discourages the development of "omnipotent" nodes that can do several tasks.
The utilization of nodes in ROS has several advantages for the entire system. Since crashes only affect certain nodes, there is more fault tolerance. Compared to monolithic systems, code complexity is decreased.

Topics

The buses that enable message exchange between nodes are known as topics and have formal and distinctive names. They implement a method for publishing and subscribing, where nodes that are configured to transmit or receive messages can act as publishers or subscribers. Anonymity policies between the nodes clearly distinguish between data producers and users. A limit amount of messages for each topic may be maintained in the queue in case they accumulate; any extra messages are not added to the queue and are lost, Wiki [36].

Services

A two-way communication tool between nodes is services. It is a method that expands on messages by giving users the option to continue listening to a particular node while also issuing commands to it in order to receive a structured response. Each service is initially documented in an.srv file, which also lists the arguments and the type of return data in addition to the name of the service. The service is represented within the server node by a function that accepts two pointers to objects of the server class as inputs: one will contain the function parameters (Request), and the other will gather the return value, Wiki [34]

Messages

The nodes of the graph exchange messages in order to communicate. These could be straightforward primitive types (such as integer, string, char, etc.) or arrays, or they could be even more complex, with structures resembling those used in C.

Bags

The method through which ROS stores logs and keeps track of all communications exchanged within a subject is represented by bags. Once a topic has been assigned to the rosbag tool, every message that is exchanged is saved in a corresponding file with the.bag extension. It is highly helpful for storing sensor data because it enables the developer to make a sort of "black box" for the robot. Additionally, ROS has a playback tool that enables graphical interface playback and visualization of the acquired data.

Master

In ROS, the master is in charge of several tasks, including adding new nodes to the network, managing the connections among the nodes in the graph, routing messages, and allowing a node to access the services of another. It is the brain of the program and can only be used by one master concurrently. If the file is implemented properly, it can be started using the roscore command or launched automatically when a node starts.

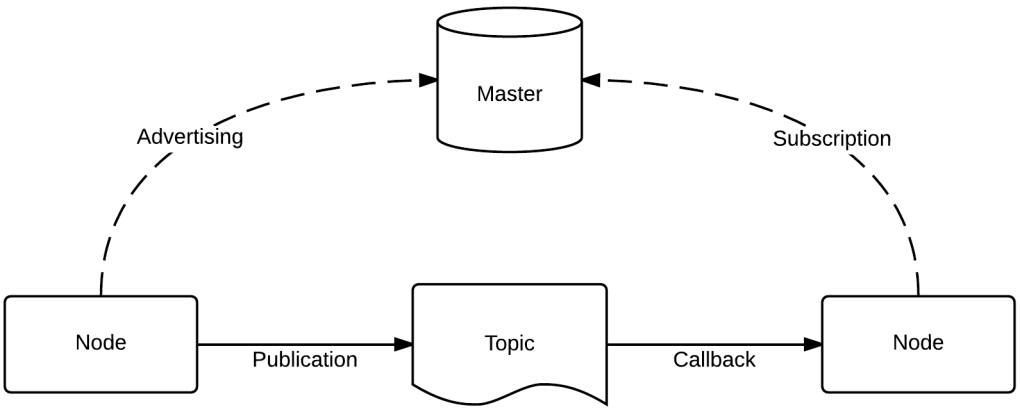

Figure 2.5: Visualization of Master-Node-Topic relationship

Parameter server

The parameter server is essentially a component of the master, allowing certain network API configurations to be shared publicly with all nodes. Although not particularly fast, it is still useful during the software testing phase. The parameters are named according to the standard ROS naming convention. This means that ROS parameters follow the same hierarchical structure as topics and nodes, Wiki [33].

Coordinate Frames and Transforms

A robot typically has numerous 3D reference systems that change over time. All of these coordinate systems are kept in a tree structure by the ROS tf package. This concept is also required to understand how URDF files handle the various parent and child links later on. As a result, the tf package keeps track of all existing relationships between point co-ordinate frames and calculates transforms between them. Developers can also use the command view frames to view the transform tree for debugging purposes.

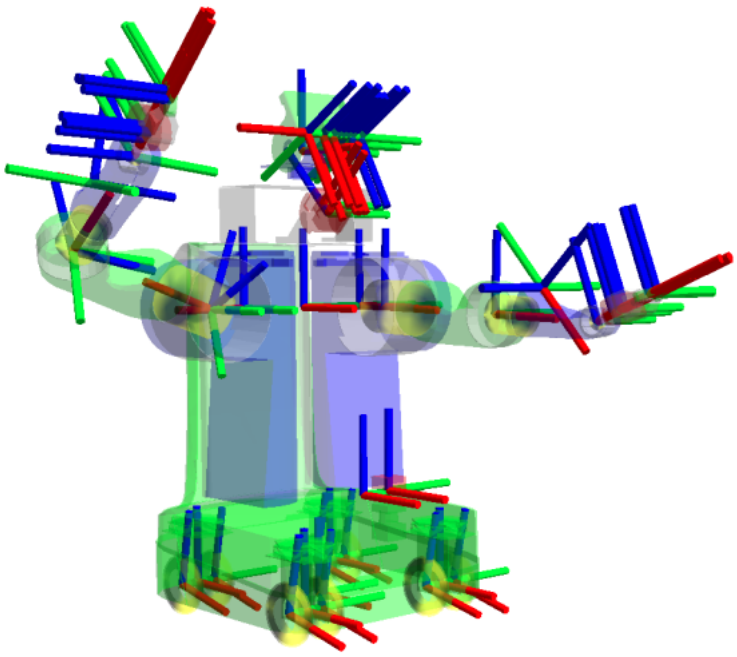

Figure 2.6: Transform Frames of a robot

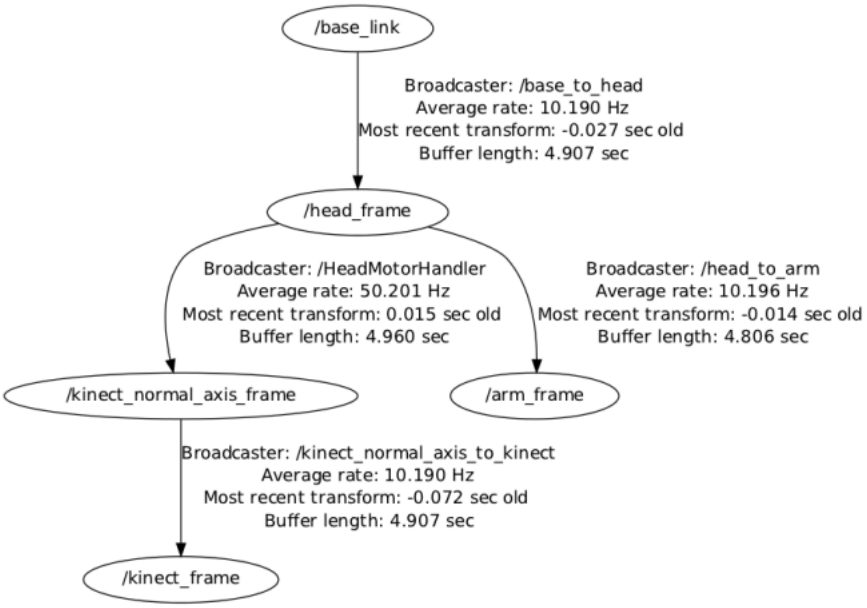

Figure 2.7: Transform Frames Tree of a robot

2.5. ROS Tools and Simulators

ROS includes built-in tools that can be used when developing robotic applications or delving deeper into certain issues. Although other tools exist, the ones described below were the ones that were used the most during the Oversonic project: RViz (3D visualization tool), Rqt (framework that enables GUI tools: Rqt graph, which displays correlation between nodes and messages in graph form, and Rqt plot), and, finally, Gazebo, a 3D simulator that has long been used in the course of this project, will be highlighted.

2.5.1. RViz: 3D Visualization Tool

RViz is a 3D visualization tool built into ROS. Its primary function is to visualize ROS messages and topics in three dimensions, assisting the user in displaying data and understanding how our system behaves. When starting a new RViz window from scratch, a black 3D scene appears. The user can indeed customize the environment by changing global options (for example, the fixed frame that provides a static reference view) and grid settings. It is possible to choose which features to display by ticking them directly from the left panel (picture 2.8). RViz can visualize topic from camera sensor, showing the images on a dedicated box. This feature applies to any kind of sensor that communicates via ROS to our robot, e.g. Lidar, tracking camera, RGB camera etc.

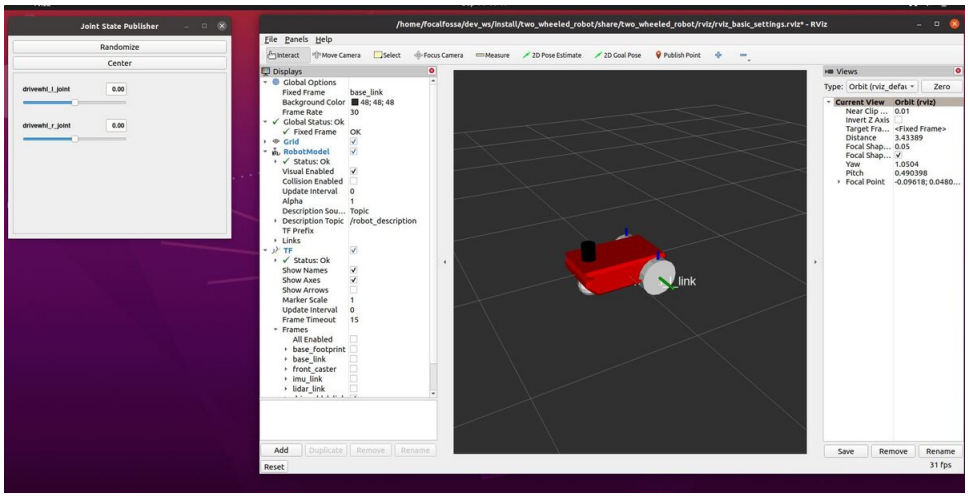

Figure 2.8: RViz GUI

2.5.2. Rqt: ROS GUI Development Tool

Rqt is a ROS software framework that implements various GUI tools as plugins. Rqt graph, in particular, is extremely useful. The primary goal of this tool is to visualize

ROS nodes, topics, and messages to aid in debugging and understanding of the system. In fact, when using ROS, it is beneficial to display the current graph in order to better understand how the various nodes communicate and how messages are exchanged. Rqt graph thus results useful in:

- Having a global overview of the system
- Debugging code in case there exist issues in nodes communication (e.g. two nodes are not connected in reality or too many nodes publish on the same topic)

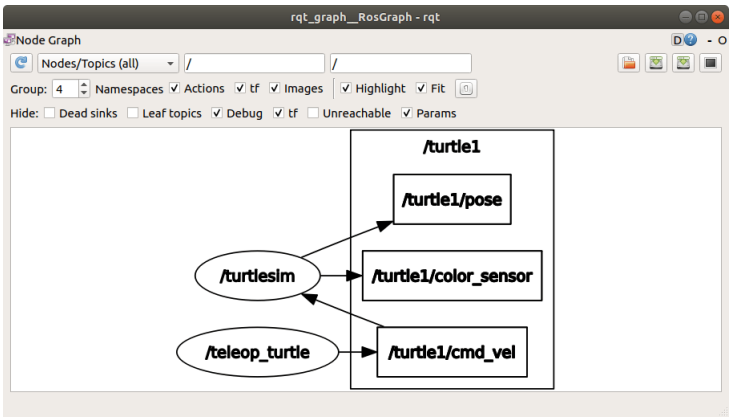

Figure 2.9: Graph from turtlesim

In figure 2.9 two nodes have been initialized and from the graph we can see the path of the messages.

2.5.3. Gazebo Simulator

Dealing with real robots means using physics labs, charging batteries, calibrating sensors and many other small tasks involving hardware. In real-life cases, even the best robots break down periodically due to human error, wear and tear or structural defects. This is where simulators come in: in simulation, we can faithfully simulate the actions that the robot will perform, without the disadvantages listed above. It is also possible to model actuators and sensors either as ideal devices or by adding varying degrees of distortion, error or failure. Thus, the solution of simulating robots in a virtual environment is efficient and cost effective. The problem of SLAM (simultaneous localisation and mapping) has always been one of the most important research topics in the community. In response to this need, 'Stages', for example, with high computational capabilities and different kinematic configurations, built-in sensors have been developed over the years. In the context of this paper, it was decided to use Gazebo, a 3D simulator that provides various

models of robots, sensors, environments, offering faithful and reliable simulations thanks to its physics engine. Gazebo is in fact one of the best-known simulators used in open source robotics.

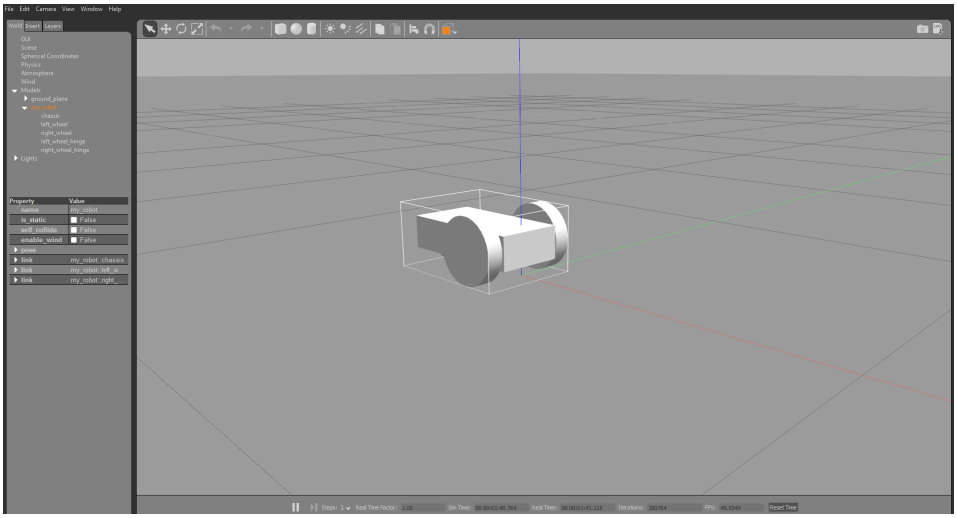

Figure 2.10: Gazebo GUI

To use the simulator, you can either download a pre-fabricated model from the Gazebo robots (such as TurtleBot, PR2, Pioneer2, and other well-known robots) or build your own robot model (we'll discuss SDF and URDF later). In terms of robots, your model can be equipped with a variety of sensors, including a stereo camera, RGB camera, tracking, and contact sensors. The noise model can also be added to the sensors. ROS is tightly integrated with Gazebo thanks to the gazebo ros package. This is a simulator plugin module that enables bi-directional communication between Gazebo and ROS. Simulated sensors and physical simulation data are thus bidirectionally transmitted between the two platforms.

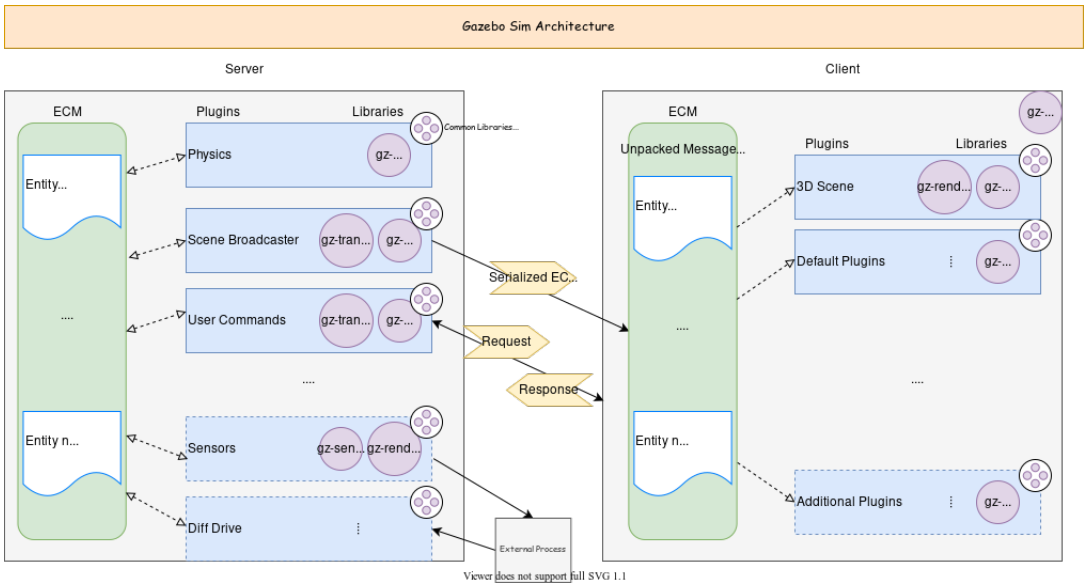

Figure 2.11: Gazebo Sim Architecture

Robot Modelling Formats

As mentioned above, one of the possible ways of describing a robot model is through the URDF. The unified robot description format is a package containing a file in XML format. A URDF file is written in such a way that each link of the robot is a child of some other parent link, with joints connecting each link. In turn, the joints are defined by an offset from the reference frame of the parent link and their axis of rotation. This creates a complete kinematics model. Below is reported a simple sample of the creation of a base link:

```
<link name="base_link">
<visual>
  <geometry>
    <cylinder length="0.6" radius="0.2"/>
  </geometry>
  <material name="blue"/>
</visual>
<collision>
  <geometry>
    <cylinder length="0.6" radius="0.2"/>
  </geometry>
</collision>
</link>
```

When we are developing complex robot models, it can happen that the notation within the XML file becomes verbose and prone to confusion. It is precisely for this reason that the XACRO (Macros XML) model was created, which is nothing more than an XML that allows the design phase of the model to be divided into sub-parts, which are then imported one by one into the main file. This results in cleaner code reading and facilitates debugging.

Below is an example of importing arguments from an external file:

```
<xacro:property name=''robotname'' value=''R001'' />
<link name=''${robotname}s_leg'' />
```

To use the model created within the Gazebo environment (which, as previously stated, works with SDFormat files), first convert from XACRO to URDF and then from URDF to SDF. In fact, files in this format include a description of the world in which the robot will be placed, a number of simulated physical world features (static and dynamic objects, lighting, terrain, and even physics), and plug-in additions. An SDF file defining a model from scratch is shown below.:

```
<?xml version='1.0'?>
<sdf version='1.9'>
  <model name='my_model'>
    ...
  </model>
</sdf>
```

3 | Robot

3.1. Introduction

«In the twenty-first century the
robot will take the place which
slave labor occupied in ancient
civilization. There is no reason at
all why most of this should not
come to pass in less than a century,
freeing mankind to pursue its
higher aspirations.»
Nikola Tesla (1856 - 1943)

«Robots of the world!
The power of man has fallen!
A new world has arisen:
the Rule of the Robots! March!»
Rossum's Universal Robot (1920)

Man has always spent his life working. Dangerous and degrading work has been the cause of death for many people for centuries. In this sense, there has always been a tendency to try to relieve man of the heaviest jobs by looking for machines or automatic systems to replace him. In a sense, with the advent of the industrial revolution, we witnessed the first real process of robotizing in history. On the other hand, with the evolution of discoveries in the medical field, the desire and curiosity arose in man to try to clone himself, artificially constructing his own like. It is here that these two needs and tendencies come together in what we now call humanoid robots. Indeed, humanoid robots are designed and built to replace humans in the most physical and repetitive tasks, in order to ensure greater well-being.

3.2. History of Robotics

In recent years, the general public has become increasingly interested in robots and robotics research. New developments, e.g. robotic competitions, which "push beyond the boundaries of current technological systems" (such as Defense Advanced Research Projects Agency (DARPA) in the United States), especially in the area of robotics, have promised and delivered fully integrated systems, Lima et al. [12].
But the idea of creating intelligent, useful machines for humans has existed since the beginning of mankind. In fact, ever since civilisation, one of the most unattainable desires and ambitions for mankind has been to create artifacts of his own image.
From a historical perspective, the first example that can be interpreted as such dates back to 3500 B.C., with the legend of the giant Talus, the slave forged by Hephaestus. Continuing in time and reaching the Babylonians in 1400 B.C., we can observe the creation of the first automatic machine, the clepsydra water clock. Continuing through the centuries, creations became more and more technologically advanced and jumping back to the 1500s, we encounter Leonardo da Vinci and his many inventions.

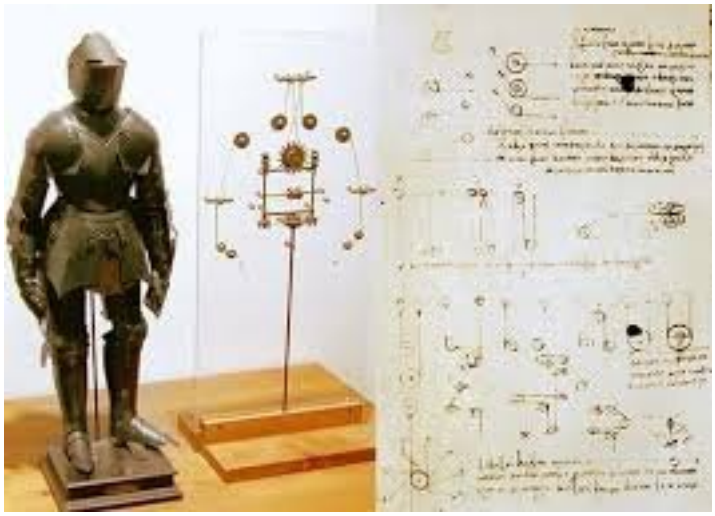

Figure 3.1: Leonardo da Vinci's mechanical knight: sketches on the right, rebuilt and showing its inner workings on the left.

The concept of the robot then gradually entered people's minds thanks to this long process, but it was only in the 20th century that it took on a real physical connotation.
The term 'robot' was introduced in 1920 by the play 'Rossum's Universal Robot', by Karel Čapek: it derives etymologically from the Slavic root word 'robota' meaning subordinate labor.

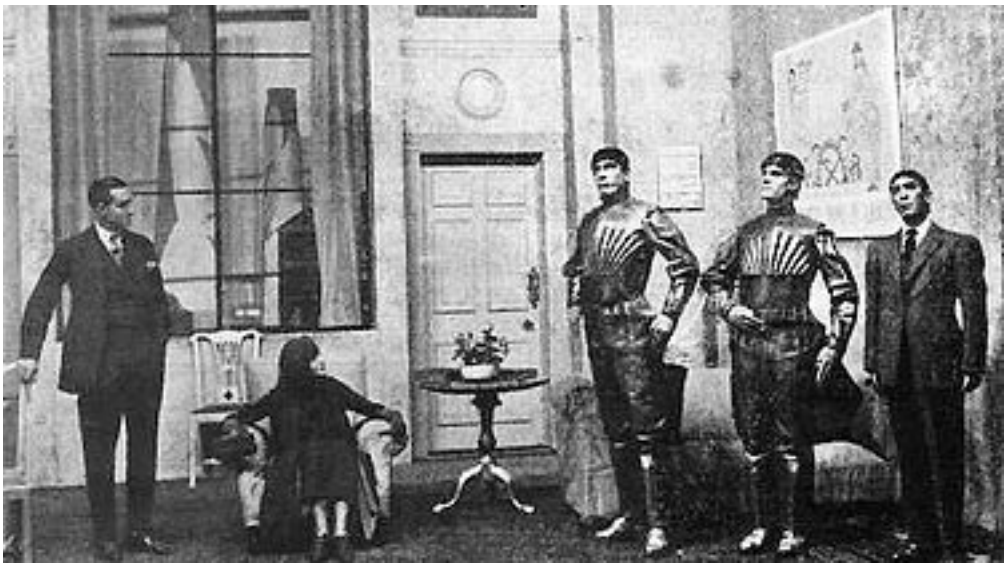

Figure 3.2: A scene from Rossum's Universal Robot play, showing three robots

Later, during the middle of the century, the first research into the connection between human and machine intelligence was undertaken, marking the beginning of Artificial Intelligence (AI). Between 1950 and 1980, Isaac Asimov wrote the so called "Three Laws of Robotics" in his book 'Runaround'. They are encoded in the "positronic brains" and are defined as follows, Asimov [2]:

- A robot may not injure a human being or, through inaction, allow a human being to come to harm.
- A robot must obey the orders given to it by human beings, except where such orders would conflict with the First Law.
- A robot must protect its own existence as long as such protection does not conflict with the First or Second Law.

Around those years, the first robots were created, they stemmed from the confluence of advances in two fields: numerically controlled machines for precision manufacturing and remote control to handle highly radioactive materials. In fact, these two fields already featured modern applications of technologies such as mechanics, control, computational science and electronics. The first robots were therefore master-slave arms, designed to reproduce the mechanics of the human arm but with rudimentary control and little perception.
During the second half of the century, the development of integrated circuits, digital computers and miniaturised components allowed terminal-controlled robots to be designed and developed.

In fact, in the 1980s, robotics was defined as the science that studies the connection between action and perception.In fact, action involves a locomotion apparatus that moves in the environment and a manipulation apparatus that performs actions, modifying its surroundings, thanks to special actuators and end-effectors.
Perception is then extracted from the sensors that provide information about the state of the robot (e.g. position and speed) and its surroundings (e.g. range and vision). In the 1990s, research was further accelerated by the need to rely on robots to replace human presence in critical environments.
As we enter the new millennium, robots have undergone profound transformations both in their scope of use and in their shapes and sizes.

Humanoid Robots

As reported in the article "Humanoid Robots: Historical Perspective, Overview and Scope", Siciliano and Khatib [23]:

"*The long saga of humanoid robots in science fiction has influenced generations of researchers, as well as the general public, and serves as evidence that people are drawn to the idea of humanoid robots. Humans generally like to observe and interact with one another. In their social behavior, people are highly attuned to human characteristics, such as the sound of human voices and the appearance of human faces and body motion.*
Infants show preferences for these types of stimuli at a young age, and adults appear to use specialized mental resources when interpreting these stimuli. By mimicking human characteristics, humanoid robots can engage these same preferences and mental resources. Throughout history, the human body and mind have inspired artists, engineers, and scientists, using media as diverse as cave paintings, sculpture, mechanical toys, photographs, and computer animation.
Humanoid robots serve as a powerful new medium that enables the creation of artifacts that operate within the real world and exhibit both human form and behavior.
The field of humanoid robotics focuses on the creation of robots that are directly inspired by human capabilities and/or selectively imitate aspects of human form and behavior. Humanoids come in a variety of shapes and sizes, from complete human-size legged robots to isolated robotic heads with human-like sensing and expression."
Thus, humanoid robots were developed to be employed as multi purpose mechanical workers, and were designed to work alongside humans in daily tasks, being a support, living in the same environment and using the same tools. It must also be considered that when the robot moves around in the work environment, there can be multiple risks for the worker;

in this respect, a subfield of robotics, called cognitive robotics, has taken hold. Indeed, robots can take advantage of the traditional communication methods used among humans to become more aware of their surroundings. An even more ambitious aim is to interpret human gestures through vision (eye gaze, body language). On the other hand, this could put a human in a difficult relationship with the robot, modelled by the phenomenon called 'uncanny valley', a concept introduced in the 1970s by Masahiro Mori, a professor at the Tokyo Institute of Technology. Masahiro in fact argues that:
"*I have noticed that, in climbing toward the goal of making robots appear human, our affinity for them increases until we come to a valley, which I call the uncanny valley.*"

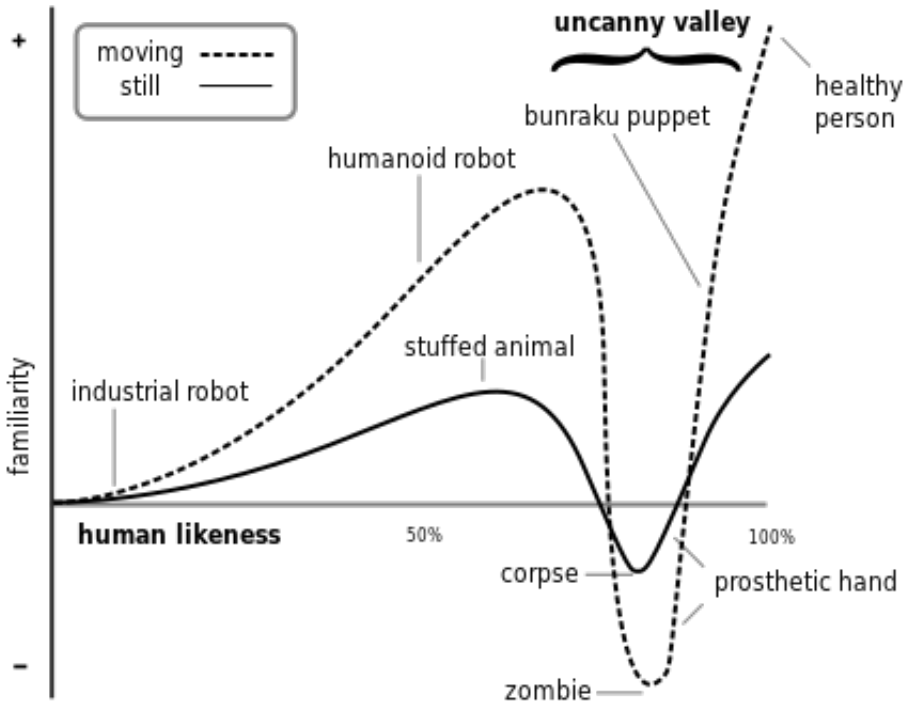

Figure 3.3: Mori Uncanny Valley

Mori better explains this concept with the example of the prosthetic hand:
"*One might say that the prosthetic hand has achieved a degree of resemblance to the human form, perhaps on a par with false teeth. However, when we realize the hand, which at first site looked real, is in fact artificial, we experience an eerie sensation. For example, we could be startled during a handshake by its limp boneless grip together with its texture and coldness. When this happens, we lose our sense of affinity, and the hand becomes uncanny.*"
On the other hand, many scientists and researchers in the robotics community see humanoid robots as a possibility to better investigate human nature itself. A part from the

roles mentioned above, a humanoid robot could work as an avatar for telepresence, test ergonomics and serve for any other roles that a human can do. Even though in the past decades, humanoids have only been applied in research field, times seem to be mature to put these robots on field and let them cooperate with humans.

3.3. Robee: Oversonic Robotics configuration

In order to make physical sense of the results obtained within this project, it is important to define what technologies were used and what materials made up Robee's hardware.

3.3.1. Hardware components and software architecture

It is important to bear in mind that the Oversonic project has an architecture split between the robot (also referred to as the edge) and the cloud, and these two components coexist in a hybrid. Describing the system from the cloud, the hardware component consists of a scalable node pool based on the 2.35Ghz AMD EPYC 7452 processor that can achieve a boosted maximum frequency of 3.35GHz with 32 GB RAM memory, running a Kubernetes instance on top of Linux Ubuntu 18.04 (Bionic Beaver). As far as the robot is concerned, all the computational power is provided by 2 Intel NUCs 8 including an Intel Core i5-8259U Processor (6M Cache, up to 3.80 GHz), 8 GB RAM and Integrated Graphics Intel Iris Plus 655. The operating system which is mounted on is Linux Ubuntu 20.04 (Focal Fossa), and all the modules are running containers that on turn are managed by KubeEdge, a containers orchestration system built on Kubernetes.

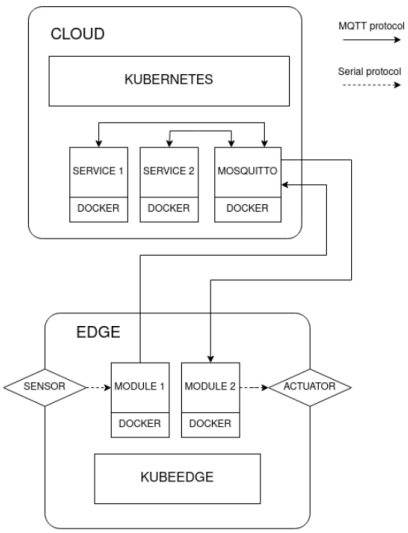

Figure 3.4: Oversonic Architecture

Internet of Things

In the case of the Robee project, the architecture is therefore composed of various software modules that are containerised and must be able to communicate with each other. The MQTT protocol is an optimal choice for this case.
From the official MQTT.org site: "*MQTT is an OASIS standard messaging protocol for the Internet of Things (IoT). It is designed as an extremely lightweight publish/subscribe messaging transport that is ideal for connecting remote devices with a small code footprint and minimal network bandwidth. MQTT today is used in a wide variety of industries, such as automotive, manufacturing, telecommunications, oil and gas*", MQTT.org [15].
MQTT therefore operates at the application layer of the OSI model, relying on TCP at the transport layer. The MQTT protocol establishes two kinds of entities in the network: a message broker and a number of clients. The broker is nothing more than a server that receives all messages from all clients and then routes these messages to the relevant destination clients. A client is anything that can interact with the broker to exchange messages. The messages are routed to clients basing on topics: every message is published over a specific topic, and only the clients subscribed to it will receive the message.
A client, therefore, can be an IoT sensor or an application in a data centre that processes IoT data. Each MQTT message has a command and a payload. The command defines the type of message:

- CONNECT: initial message sent from client to broker, to instantiate a new connection
- DISCONNECT: final message sent from client to broker to end the connection
- PUBLISH: command to publish a message over a specified topic, it is sent from client to broker and then routed from broker to every client that appears to be subscribed to that topic
- SUBSCRIBE: message sent from client to broker in order to request a subscription to a specified topic

All MQTT libraries provide simple ways to handle such messages directly and can automatically populate certain required fields, such as 'message' and 'client Id'.

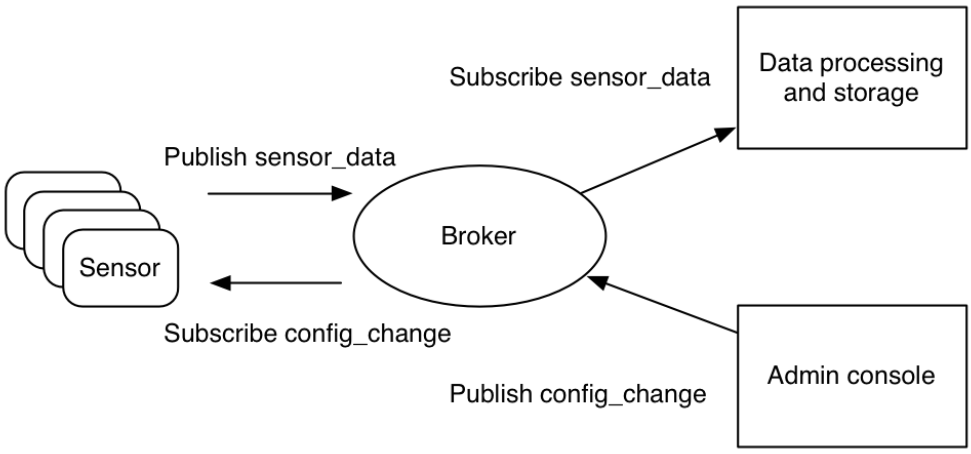

Figure 3.5: The MQTT publish and subscribe model for IoT sensors

3.3.2. Robots Configurations

The robots covered by the work in this thesis are mainly three

- R007 is a small autonomous mobile robot used by Oversonic as a prototype in the testing phase and features skid steering kinematics. In fact, it has two belts with two torque motors. The system is based on an Intel NUC and peripherals: two or four lidar sensors, a tracking camera and a depth camera mounted on the top base. The use of this AMR (autonomous mobile robot) is mainly conceived in conjunction with its larger 'brother' Robee or in industrial logistics environments.

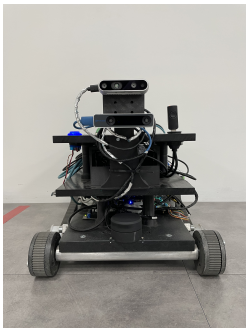

Figure 3.6: R007

- R012 is the humanoid robot developed in Oversonic Robotics, now in its fourth evolution from the initial prototype and featuring a differential drive base. The system is divided into two parts, a lower body and an upper body, each featuring an NUC terminal and several sensors, but in this analysis we will focus exclusively on the lower part. The lower body in fact contains within it the two torque motors, which move two wheels actively. For the robot's stability, two passive caster wheels have been added to the front and rear of the base. Two Lidar sensors are then mounted on the base and going up about halfway up the torso are a tracking and depth camera.

Figure 3.7: Robee R012

- N002 is a robot used for the testing phase of Robee's lower body. It has a similar purpose of use to R007. It has a differential drive base with two torque motor actuators, like R012 but with a physical arrangement of peripheral sensors but only one NUC.

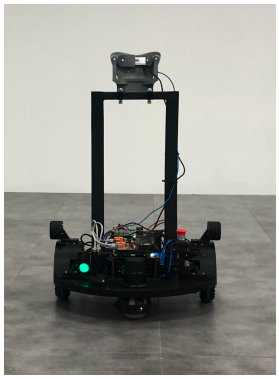

Figure 3.8: N002

The main features of the skid steering and differential drive kinematics will be listed.

Skid Steering

Skid Steering is a particular kinematics configuration featuring two tracks. It is composed of two tracks on its basic configuration, left and right, and the control variables are indeed left and right speed. Another configuration entails a 4 wheels set up featuring a low wheelbase configurations so that they can be deemed as two tracks. When rotating the central point does not move as the track is sliding on the ground. It is clear that this drive needs proper calibration and slippage modeling in order to be reliable. Some assumptions are needed for this kinematics model: the first, mass is placed in center of the fictitious medium, the second, all the wheels on the same side have the same speed. While in motion, this kind of drive presents multiple ICR and all of them share the same ω_z.

$$\begin{bmatrix} v_x \\ v_y \\ \omega_z \end{bmatrix} = J_\omega \begin{bmatrix} \omega_l r \\ \omega_r r \end{bmatrix} \tag{3.1}$$

The wheels are turning and sliding simultaneously, resulting in two fictitious instantaneous centers of rotation: ICR_{left} and ICR_{right}. Under proper assumptions, skid-steering can be simplified to a differential drive kinematics.

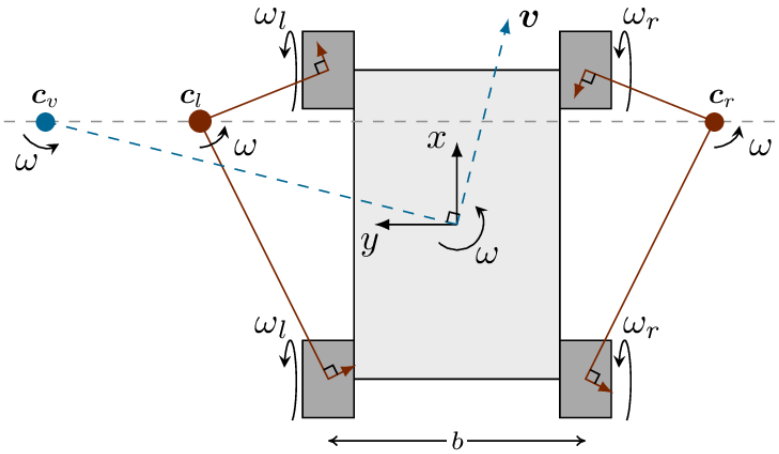

Figure 3.9: Skid Steering Kinematics

Under proper assumptions, skid-steering can be simplified to a differential drive kinematics.

Differential Drive

Differential drive configuration present the following construction:

- two wheels working on the same axis
- two independent motors, one for each wheel
- one or two passive caster wheels

Control input in this case are the linear and the angular velocity of the robot, v and ω. Wheels move around an Istantaneous Centre of Rotation on a circular path with istantaneous radius R and angular velocity ω.

$$\begin{bmatrix} x' \\ y' \\ \theta \end{bmatrix} = \begin{bmatrix} \cos\omega\delta t & -\sin\omega\delta t & 0 \\ \sin\omega\delta t & \cos\omega\delta t & 0 \\ 0 & 0 & 1 \end{bmatrix} \begin{bmatrix} x - ICR_x \\ y - ICR_y \\ \theta' \end{bmatrix} + \begin{bmatrix} ICR_x \\ ICR_y \\ \omega\delta t \end{bmatrix} \tag{3.2}$$

It is therefore possible to reconstruct robot pose from direct kinematics:

$$x(t) = \frac{1}{2}(\int_0^t (V_R(t') + V_L(t'))\cos\theta(t')\,dt') \tag{3.3}$$

$$y(t) = \frac{1}{2}(\int_0^t (V_R(t') + V_L(t'))\sin\theta(t')\,dt') \tag{3.4}$$

$$\theta = \frac{1}{b}(\int_0^t (V_R(t') - V_L(t'))\,dt') \tag{3.5}$$

where V_R and V_L are defined as follows:

$$V_R = \omega(R + \frac{b}{2}) \tag{3.6}$$

$$V_L = \omega(R - \frac{b}{2}) \tag{3.7}$$

and as a consequence the following is derived:

$$V = \frac{V_R + V_L}{2} \tag{3.8}$$

$$\omega = \frac{V_R - V_L}{2} \tag{3.9}$$

It becomes clear that we can compute robot odometry by integrating the so-called control variables and knowing the parameters of the wheels, namely the direct kinematics. On the contrary, we can derive control variables from a desired pose or velocity.

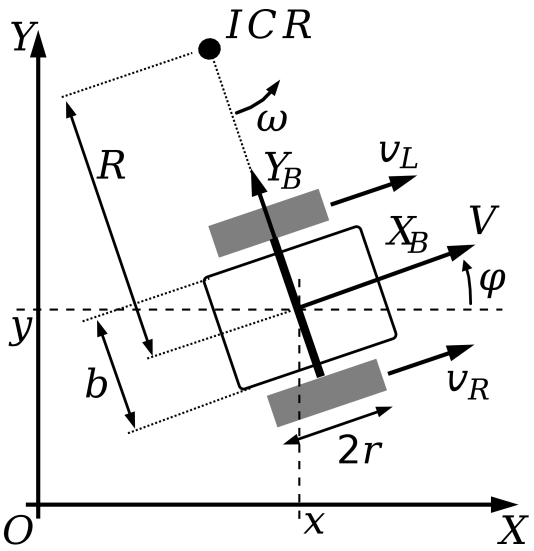

Figure 3.10: Differential Drive Kinematics

It is interesting to mention three borderline cases for this kind of drive:

- $V_L = V_R$: forward linear motion is straight
- V_L = - V_R: rotation in place
- $V_L = 0$ or $V_R = 0$: respectively, rotation about left and right wheel

3.3.3. Sensors

In order for a robot to perceive the world around it and to complete tasks autonomously, sensors are required. We distinguish between proprioceptive (internal state of the robot) and exteroceptive (state of the external environment) sensors. In this section, we focus on the exteroceptive sensors that have been used in Robee, providing a brief overview of their functioning.

D400 Intel Depth Camera

Depth cameras are a type of sensor widely used in robotic applications. They normally consist of two parts: a traditional digital camera, which captures RGB data, and a projec-

tor, which captures depth data.The depth system can work in several ways, for example by projecting a grid of light structured in a non-visible spectrum into a scene and then analysing the distortion created in this pattern to determine the distance and/or shape of any object placed in front, Jonasson et al. [10]. In our application, the main reason for using the d455 camera in Robee's lower body is ????distance measurement?????. Traditional digital cameras shoot out an image as a grid of pixels in two dimensions. Each pixel is then associated with three values ranging from 0 to 255, which define the red, green and blue components, so black, for example, is (0,0,0) and a pure bright red would be (255,0,0). . This type of representation is called an RGB image. Thus, each image is composed of three channels each storing the values pertaining to each colour component.

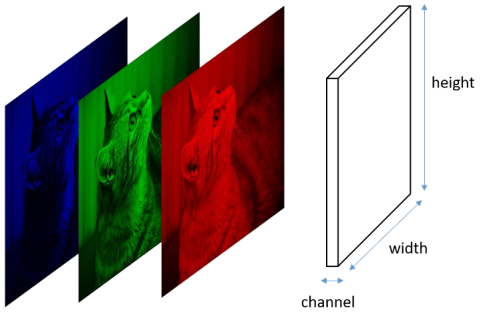

Figure 3.11: Channel decomposition

In the case of a depth camera, on the other hand, the pixels have different numerical values associated with them, where the number represents the distance of the corresponding pixel from the camera, thus the depth. Thus, by unifying this representation we will have a colour map where cooler colours represent closer obstacles, and warmer colours represent more distant obstacles, in depth.

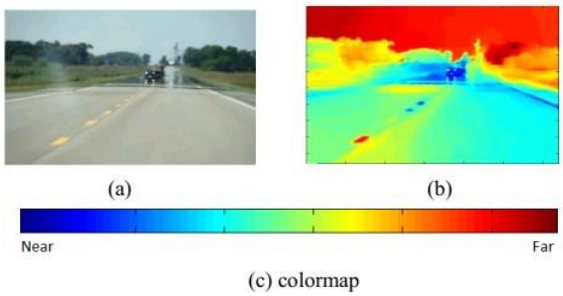

Figure 3.12: Depth-map representation

Figure 3.13: D455 Intel Tracking Camera

Therefore, there are two types of three-dimensional image formats, the first being RGB-D and the second being pointcloud. The first has already been introduced above, and we recall that for each pixel, identified by the coordinates (x,y), four properties (R,G,B,depth) are associated. The substantial difference between the point cloud and RGB-D data is that in the pointcloud, the coordinates (x,y) represent the real world value instead of integer values. When viewing the two types of data, in fact, the former is presented in a sparse structure, while the latter is based on grid-aligned images. A practical application of point cloud will be provided in chapter 6

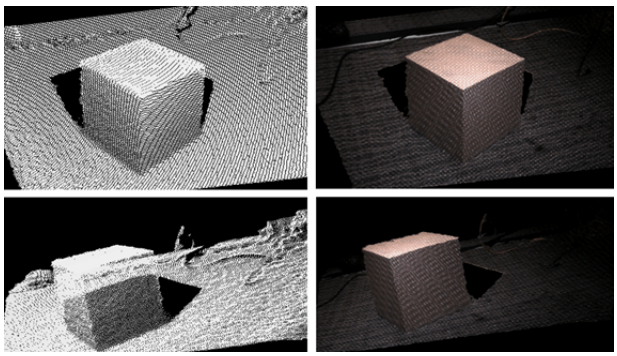

Figure 3.14: Point Cloud sample

Thus, the point cloud can be constructed from RGB-D format images. In fact, by knowing an RGB-D dataset and the camera's intrensic values through a process called camera calibration. Since pointclouds are sets of disordered vectors, it is common for researchers to change the structure of the pointcloud data into 3D voxel grids. The voxel grid geometry is in fact a grid of values in three dimensions, organised in layers of rows and columns. The reason for this conversion also comes from the fact that one often then has to deal with deep learning models that expect highly regular input data formats.

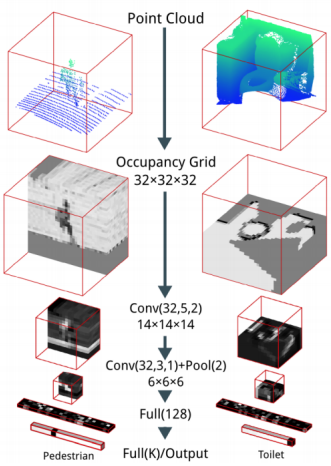

Figure 3.15: Voxel Grid example: A 3D Convolutional Neural Network for Real-Time Object Recognition

T265 Intel Tracking Camera

The T265 tracking camera is designed to integrate odometry data from the robot. It is in fact an independent and robust support for visual-inertia odometry and re-localisation. A key strength of visual-inertial odometry is that the various sensors available complement each other. The images from the visual sensors are supplemented by data from an onboard inertial measurement unit (IMU), which includes a gyroscope and accelerometer. The aggregated data from these sensors is fed into simultaneous localization and mapping (SLAM) algorithms. The tracking is done by comparing the information collected by the two fish-eye cameras, which collect images at 30 fps, Intel [9].

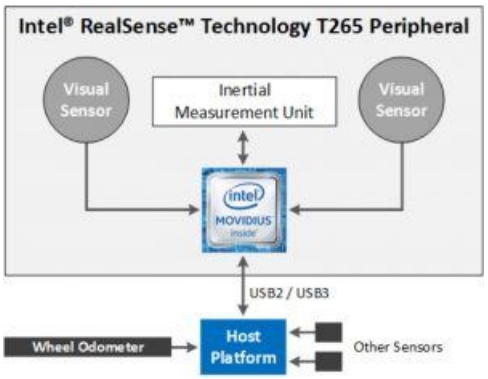

(a) Block diagram of Intel T265

(b) T265 Intel Tracking Camera used in Robee

YDLidar

LiDAR (Light Detection And Ranging) identifies technology that measures the distance to an object by illuminating it with laser light, while at the same time being able to return high-resolution three-dimensional information about the surrounding environment. A LiDAR typically uses several components: lasers, photodetectors and readout integrated circuits (ROICs) with time-of-flight (TOF) capability to measure distance by illuminating a target and analysing the reflected light.

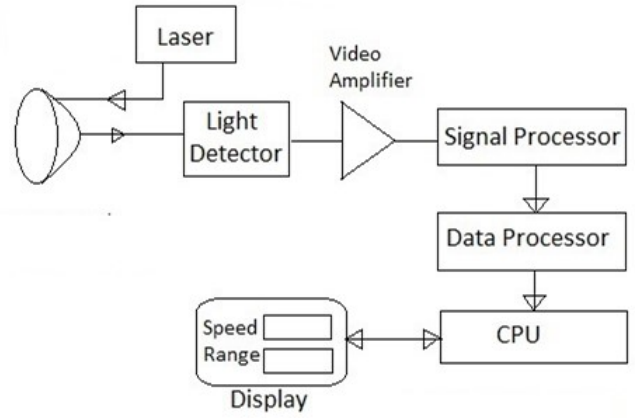

(c) Lidar architecture

(d) Ydlidar model G4 used in Robee

YDLIDAR G4 is a 360-degree two-dimensional rangefinder developed by YDLIDAR. Based on the principle of triangulation, it is equipped with related optics, electricity, and algorithm design to achieve high-frequency and high-precision distance measurement. The mechanical structure rotates 360 degrees to continuously output the angle information as well as the point cloud data of the scanning environment while ranging. YDlidar provides a built in bridge to ROS that ease the integration with the overall system.

Item	Min	Typical	Max	Unit
Ranging Frequency	/	9000	/	Hz
Ranging distance	0.12	/	16	m
	0.26	/	16	m
	0.28	/	16	m
Field of View	/	0-360	/	Deg
Angle Resolution	0.2 at 5 Hz	0.28 at 7 Hz	0.48 at 12 Hz	Deg

Table 3.1: Specifications for Ydlidar G4

Visual Fiducial System

During the use and development of Robee's navigation, so-called Apriltags were used, a particular visual fiducial system chosen for its robustness and integration with the simulated Gazebo environment. Visual fiducials are nothing more than artificial landmarks, designed to be easily recognisable within the working environment and distinguishable from one another. The methodology is similar to that of a common QR code but with significant applications and objectives. In fact, unlike a QR code, where the user has to frame the tag with the camera and capture the high-resolution snapshot, these types of tags are designed to work with a small amount of information (even as little as 12 bits) but with performance and ease of use that is clearly superior to QR codes. In fact, these types of tags are designed to be automatically detectable and localisable even in low resolution conditions, even providing the relative position and orientation of the tag with respect to the camera. In terms of size, the Apriltags used range from 50 to 100 pixels, including the payload, Olson [18].

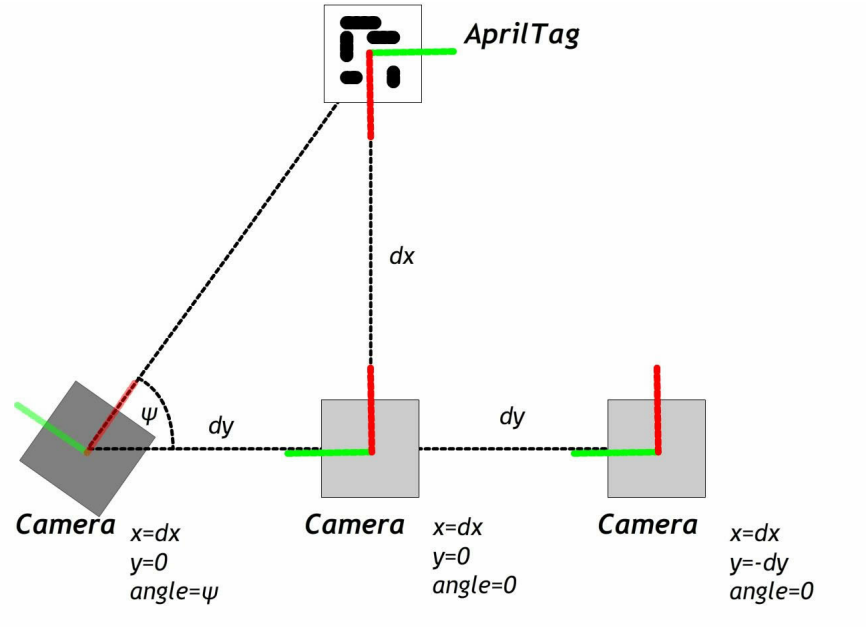

Figure 3.16: AprilTag distance and orientation measurement

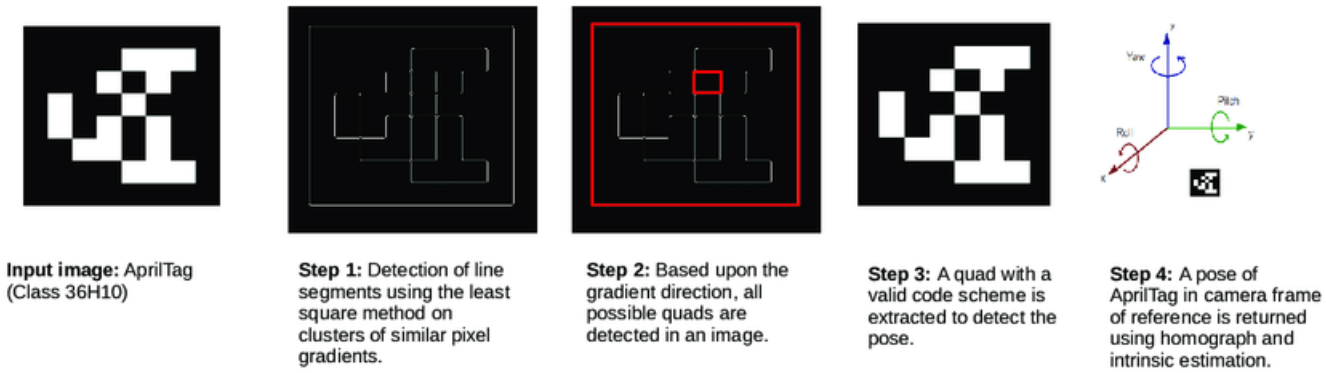

Figure 3.17: How AprilTag detection is performed

Visual fiducial systems have been used in robotics to improve human/machine interaction, enabling the development of commands such as 'follow me'. In the context of this work, tags were used for SLAM (Simultaneous Localisation and Mapping), as an independent support to the sensors mentioned in the previous section. In fact, in both the simulated and real environment, tags were placed in strategic positions in order to reposition the robot to the correct pose by comparing the information coming from the sensors and that coming from the tags. AprilTag provides a package for perfect ROS integration.

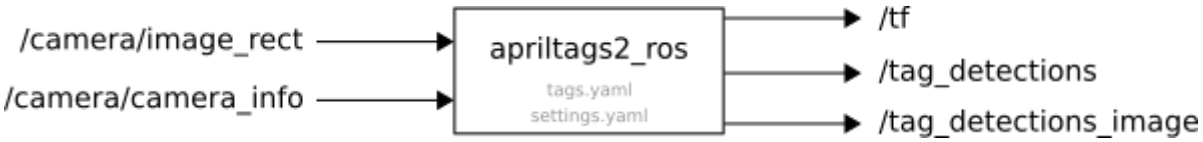

Figure 3.18: ROS TF

The apriltag ROS package then takes as input the topic of the rectified image and returns a list of recognised tags and their positions in 3 dimensions. However, in order to work, one must specify in the configuration files (settings and tags) which tag families to search for. A practical application will be provided in chapter 5

Indoor Positioning System

For the purpose of this thesis, another technology that has been used is the Indoor Positioning System. This is in fact a new approach to the problem of localisation when remote GNSS satellites, which are commonly blocked indoors, are not available. There is now a wide offer for this type of solution, even with different communication protocols at its base: from Wi-Fi signals to Bluetooth to ultrasound. In Robee, the choice was made to use an IPS system provided by Marvelmind, which is based on ultrasonic and

time-of-flight (ToF) measurements with trilateration, yor [1], and which also provides for communication via ROS topics, thus providing integration with the robotics platform used. The system proposed by Marvelmind consists of a series of static beacons (four were used in our case), placed on the walls of the production area of Oversonic Robotics.

Figure 3.19: MarvelMind beacons kit

Each beacon sends and receives a stream of hypersonic signals continuously. There is also a modem, which is connected to the PC on which the supplied software is run, and a beacon called a 'hedgehog' which is placed on the vehicle to be located, in this case Robee. The hedgehog then receives the signals from the four beacons and sends them to the modem, which proceeds to triangulate. The communication frequency is customisable and directly affects localisation accuracy, which in the basic configuration is claimed to be +/- 2 cm.

4 | Navigation Stack

4.1. Introduction

In this chapter, we will address SLAM (simultaneous localization and mapping) and navigation techniques used in this thesis. We will focus exclusively on the literature overview of techniques used in practice, without comparing the various existing approaches. We will therefore overview all the components of the see-plan-act architecture. The sense-plan-act architecture in fact explains the entire process that starts from the map building, to the global and local planning up to sensor fusion. It is indeed composed of:

- Map
- Sensors
- Current Position
- Goal Position
- Trajectory Planning
- Trajectory Following and Obstacle Avoidance

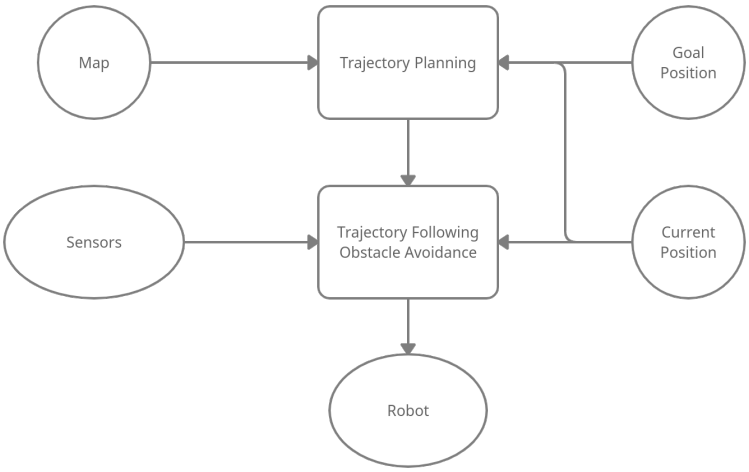

Figure 4.1: Block scheme representation of sense plan act architecture

4.2. Simultaneous Localization and Mapping

In this first subsection we will focus on map side, understanding how maps are build, interpreted and how the agents localize inside the map. There exists two main types of representing a map:

- Landmark-based: a particular type of representation, mainly used for localization, that is based on detecting landmarks. This technique results in a sparse representation of the space, leaving much to the unknown;
- Grid maps: the map results in a discredited version of the environment, where each cell contain information about occupation/non occupation/unkwown. It results in a very dense representation where almost the totality of the cells are caught.

In the scope of this work we will focus on occupancy grid map.

4.2.1. Occupancy Grid Map

As anticipated, occupancy grid map is a peculiar map representation that attempts to discretize the continous environment into a two dimensional grid map. The grid map is again divided into array cells of size from 5 to 50 cm and each of them hold a probability value that stands for the likelihood to be free or occupied. Thus, occupancy grid maps try to solve the problem of reconstructing consistent maps from noisy and uncertain measurement data, under the hypothesis of knowing the robot pose. The reasoning behind most occupancy grid mapping algorithm is to calculate the posterior over maps, given the data, in a probabilistic way.

$$p(m|z_{1:t}, x_{1:t}) \tag{4.1}$$

where m is the map,$z_{1:t}$ is the set of measurements up to time t and $x_{1:t}$ the set of all the poses taken by the robot, namely its path. Being m_i the i-th grid cell and having it a binary occupancy value that states if a cell is free or occupied (1 for the cell being occupied, 0 free), we can define:

$$m = \sum_i m_i \tag{4.2}$$

.

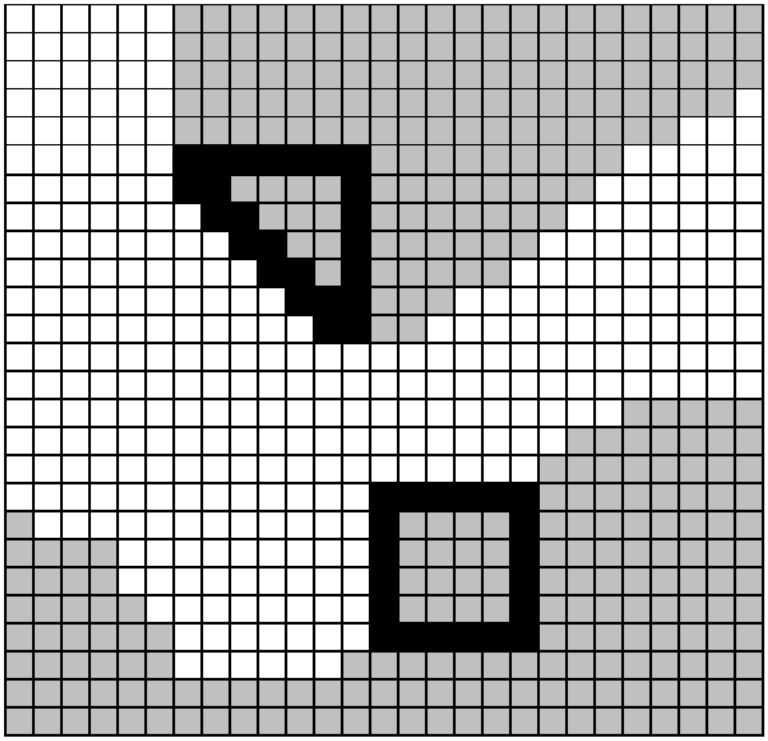

Figure 4.2: Sample of an Occupancy Grid

Due to the curse of dimensionality, the probabilistic approach reduces to estimate the single cell occupancy rather than the entire map:

$$p(m_i|z_{1:t}, x_{1:t}) \tag{4.3}$$

To calculate the single cell occupancy we resort to Bayes rule:

$$p(m_i|z_{1:t}, x_{1:t}) = \frac{p(z_t|m_i, z_{1:t-1}, x_{1:t})p(m_i|z_{1:t-1}, x_{1:t})}{p(z_t|z_{1:t-1}, x_{1:t})} \tag{4.4}$$

Additionally recurring to Markov assumption, stating that the current state depends on only a finite fixed number of previous states, measurement z_t depends only on x_t and m_i. It is common use at this point to adopt log-odds representation of occupancy, as to avoid being with probabilities close to 0 and 1:

$$l_{t,i} = \log \frac{p(m_i|z_{1:t}, x_{1:t})}{1 - p(m_i|z_{1:t}, x_{1:t})} \tag{4.5}$$

The process loops and assumes the form of the algorithm 4.1. It is important to note that

only the cells which fall under the sensor cone of measurement are updated through the inverse sensor model, Thrun et al. [26].

Algorithm 4.1 Occupancy Grid Algorithm

```
Algorithm occupancy grid mapping(l_{t-1,i}, x_t, z_t)
for all cells m_i do
  if m_i in perceptual field of z_t then
    l_{t,i} = l_{t-1,i} + inverse_sensor_model(m_i, x_t, z_t - l_0)
  else
    l_{t,i} = l_{t-1,i}
  end if
end for
return l_{t,i}
```

where the inverse sensor model is defined as follows:

$$inverse\_sensor\_model(m_i, x_t, z_t) = p(m_i|z_t, x_t) \tag{4.6}$$

The motivation for the "inverse" denomination is because it reasons from effects to causes: it provides an information about the world where that same information was derived from a measurement caused by the world it self:

$$p(m_i|z_{1:t}, x_{1:t}) = \eta \int m : m(i) = m_i p(z|x, m)p(m)dm \tag{4.7}$$

A function approximator has to be used, since this algorithm cannot be computed due to the large map space.

4.2.2. SLAM algorithm

At this point we turn to the problem of SLAM, Simultaneous Localisation and Mapping. This stems from the robot's need to map a new environment, of which nothing is known, and at the same time to localise the robot itself within the map being created. The problem is particularly difficult as one does not have access to the robot's poses and uncertainty is kept on all the components. Moreover, it proposes to correct both odometry and uncertainty of estimated position and landmark. Two approaches to SLAM can be defined, from a probabilistic point of view:

- Full SLAM: simultaneous estimate of path and map
- Online SLAM: simultaneous estimate of the most recent pose and map

Full SLAM Full SLAM addresses the problem of estimating the joint probability of the entire trajectory and landmark.

$$p(x_{1:t}, m|z_{1:t}, u_{1:t}) \tag{4.8}$$

For this purpose we propose a significant example: FastSLAM. Fast Simultaneous Localization and Mapping uses a sampled particle filter distribution model, solving the full SLAM problem. If we consider the full trajectory X_t rather than a single pose x_t, the following holds:

$$p(X_t, m|z_t) = P(X_t|z_t)P(m|X_t, z_t) \tag{4.9}$$

where $P(X_t|z_t)$ is the estimate of the trajectory and $P(m|X_t, z_t)$ is the estimate of the map given the trajectory. Thus, in FastSLAM the trajectory X_t is represented by particles $X_t(i)$ while the map is represented by a factorization called Rao-Blackwellized filter. The approach so is to treat each pose particle as it it was the entire trajectory, processing all of the feature measurements independently.

$$P(m|X_t^{(i)}, z_t) = \prod_{j}^{M} P(m_j|X_t^{(i)}, z_t) \tag{4.10}$$

Indeed, once the trajectory is known, all of the features become uncorrelated.

$$p(x_{1:t}, l_{1:m}|z_{1:t}, u_{0:t-1}) = p(x_{1:t}|z_{1:t}, u_{0:t-1})p(l_{1:m}|x_{1:t}, z_{1:t}) \tag{4.11}$$

where we have SLAM posterior, robot path posterior and landmark positions respectively. Previous equation can be simplified by factorization as follows:

$$p(x_{1:t}, l_{1:m}|z_{1:t}, u_{0:t-1}) = p(x_{1:t}|z_{1:t}, u_{0:t-1}) \prod_{i=1}^{M} p(l_i|x_{1:t}, z_{1:t}) \tag{4.12}$$

In this way the dimension of state space is reduced making particle filtering possible:

$$O(N \times \log(M)) \tag{4.13}$$

with N being the number particles and M the number of map features

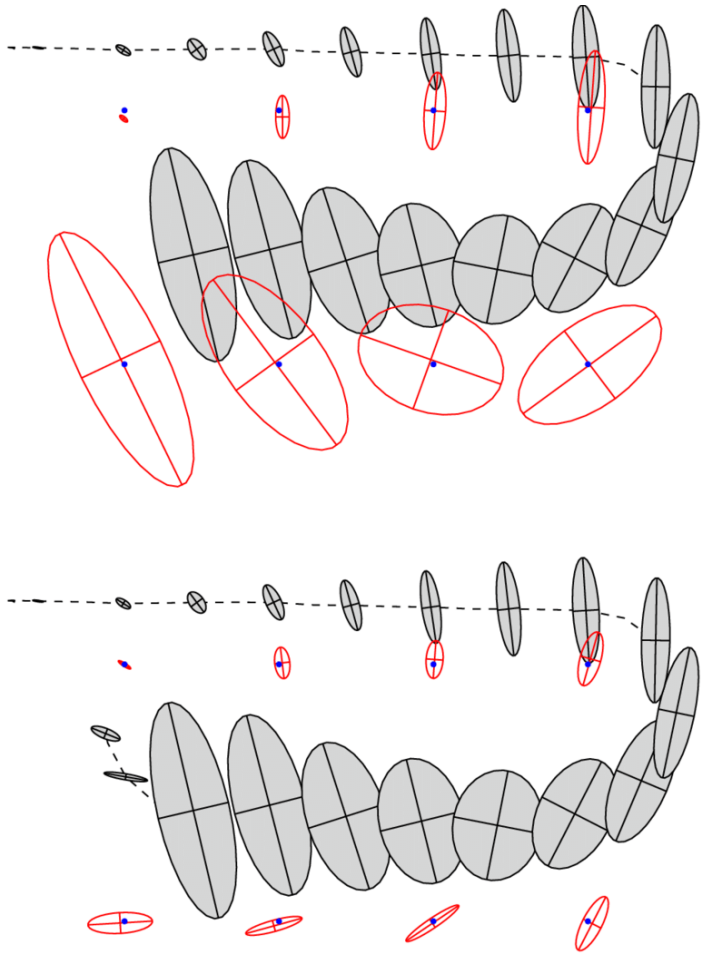

Figure 4.3: SLAM problem: initial uncertainty on pose and consequent decrease thanks to previously seen landmarks, Thrun et al. [25]

Summarizing, FastSLAM adopts a Rao-Blackwellized particle filtering based on landmarks, Montemerlo et al. [14], where each particle is a trajectory, each landmark is represented by a 2x2 EKF and therefore each particle has to maintain M EKFs.

Online SLAM Online SLAM entails estimating the posterior over the last pose along with the map: $p(x_t, m_i|z_{1:t}, u_{1:t})$ where x_t is the pose at time t, m is the map, $z_{1:t}$ $u_{1:t}$ the measurements available up to time t. The fact that we refer to this technique as online SLAM directly derives from the fact that we're considering data at time t, estimating last pose only.

$$p(x_t, m|z_{1:t}, u_{1:t}) = \int \int ... \int p(x_{1:t}, m|z_{1:t}, u_{1:t}) dx_1 dx_2 ... dx_{t-1} \tag{4.14}$$

As one can notice, the online SLAM problem is the result of integrating out one at

a time past poses from the full SLAM problem. A significant example of a proposed solution to Online SLAM is proposed: EKF SLAM. Extended Kalman Filter Simultaneous Localization and Mapping uses a linearized Gaussian probability distribution.

Algorithm 4.2 Extended Kalman Filter

Extended Kalman filter$(\mu_{t-1}, \Sigma_{t-1}, u_t, z_t)$
μ' = g(u_t, μ_{t-1})
Σ_t' $= G_t \Sigma_{t-1} G_t^T + R_t$
$K_t = \Sigma'_t H_t^T (H_t \Sigma'_t H_t^T + Q_t)^{-}1$
$\mu_t = \mu'_t + K_t(z_t - h\mu_t)$
$\Sigma_t = (I - K_t H_t)\Sigma'_t$
return μ_t, Σ_t

EKF-SLAM promises good performances but it has two main drawbacks: it employs linearized models of non-linear motion and observation models, inheriting many caveats; it is computationally demanding. One possible solution to this problem is the above reported FastSLAM (Rao-Blackwellisation filter).

4.2.3. SLAM Toolbox

During the experience at Oversonic Robotics, the SLAM toolbox was chosen for the simultaneous localisation and mapping problem, though many predecessors exist. The ROS packages responsible of SLAM can be divided into Bayes-based filter implementations, like GMapping and HectorSLAM, and graph-based implementations, as Cartographer and Karto SLAM. The SLAM Toolbox package is an open source software developed by Steve Maceski which use graph based approach and occupancy grid map. It has been widely used on the various ROS distros and has become the default SLAM algorithm for ROS2. It arose from the need to build accurate maps of large environments, where previous SLAM tools had shown shortcomings.
SLAM Toolbox provides three operating modes, Macenski and Jambrecic [13]:

- Synchronous Mapping: provides the ability to map and localize in an environment while keeping a bunch of measurements to be added to SLAM. This results useful when the quality of the map is important.
- Asynchronous Mapping: on the contrary, this mode manages new measurements only when previous measurement has been completed. This makes this modality useful when real time localization is crucial.
- Pure Localization: cannot detects changes in the space. It tries to match a local bunch of measurements with the data originally gathered.

4.2.4. Advanced Monte Carlo Localization

The pose estimation used in Oversonic applications is based on AMCL pose (Advanced Monte Carlo Localization). This technique relies on the so called particle filter approach. An extremely large number of particles covering the entire state space are used to initialize particle filters. The robot has a multi-modal posterior distribution because it predicts and update the measurements as it obtains more measurements. A Kalman Filter approximates the posterior distribution to be a Gaussian, which is a significant departure from this. The particles converge to a single value in state space after several rounds. Maintaining the random distribution of particles over the state space is a major challenge for particle filters, which becomes impossible for large dimensional problems. These factors make an adaptive particle filter far superior to a simple particle filter in terms of convergence speed and computational efficiency.

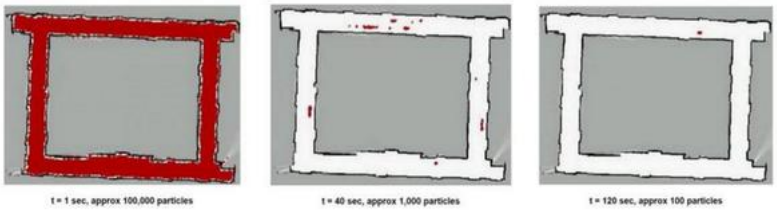

Figure 4.4: Particle Filter in Action over Progressive Time Steps, Base [3]

The main concept is to limit the inaccuracy caused by the particle filter's sample-based representation. The real posterior is thought to be represented by a discrete, piecewise constant distribution, such as a discrete density tree or a multidimensional histogram, in order to calculate this bound. We start with a map of our surroundings when using an adaptive particle filter for localization, and we can either manually localize the robot by setting it to a certain point or we may make the robot start from with no initial estimate of its position. We now create new samples that forecast the robot's position following the motion command as it advances. By re-weighting these samples and leveling the weights, sensor readings are included. In general, it is a good idea to add a few random, evenly dispersed samples because they aid in the robot's recovery when it loses track of its location. Without these random samples, the robot will continue to resample from the erroneous distribution under those circumstances and will never recover. We could encounter dis-ambiguities inside a map due to symmetry in the map, which is what gives us a multi-modal posterior belief, which is why it takes the filter many sensor readings to converge.

4.3. Global Planning

Mobile robots are meant to move from their current positions to some goal inside the map. Once that the SLAM task has been performed and a map has been obtained, we can address the This is known as trajetory planning and it is managed by the so-called global planner. Robot motion planning goals are:

- collision-free trajectories
- most efficient or most optimal (depending on the chosen optimality criterion) trajectory

The problem that global planner addresses regards finding a collision free path between an initial pose and the goal, taking into account the existing constraints. It is important to distinguish between some concepts used in this scope:

- Path: a geometric locus of way points
- Trajectory: a path for which a temporal law is specified
- Manouver: a series of actions that a vehicle should execute

In the scope of this thesis we are going to analyze a path planning algorithms, the so-called A*. This algorithms is part of the graph based planning family. The underlying idea is to construct a discretized representation of the map, building a graph out of it (4 or 8 neighbors connectivity are possible) and eventually searching for the shortest path in the graph, namely the optimal solution. It is relevant to report that the resolution of the grid directly influences the accuracy of the plan: a more dense resolution will describe in a more complete way the map it is investigating, thus resulting in a deeper analysis of the possible paths.

(a) a (b) b

Figure 4.5: Comparison of 4 connectivity (a) and 8 connectivity (b)

This connectivity scheme reproduces on a grid the kinematics motion a robot is supposed to do in reality, so that performing the path search on the grid is representative of how the robot would move in reality. The usual approach to search graphs for the optimal path

4.3.1. A* algorithm

The A* algorithm was developed on the basis of the Dijkstra algorithm m improving its performance and is therefore one of the most widely used in path finding and graph traversal today. The components of this algorithm are the two points (start and end point), the grid and the nodes. In this approach what is important is the cost of moving from one edge to the others. The predecessor of A*, Dijkstra algorithm, in fact focuses on the idea of cost: each part of the path has an intrinsic cost and the algorithm visits all of the existing edges trying to lower the overall cost. The algorithm manages a queue list where it keeps all the nodes that are still to analyzed, where the nodes with the smallest distance to the starting point is the first node in the queue, Herzog [8]. Every time we move to some node, we encounter other nodes that previously were unaccessible, since we are dealing with k connectivity framework, and if these nodes are still to be traversed they are added to queue. This process ends as soon as the priority queue is emptied, namely when there are no nodes left to be investigated. Every time the algorithm shifts to some new node it records the path that led to that node and the specific costs, so the shortest path to each node can be computed by going backwards in the path. A* is based on the best first search speeds up this process by splitting the cost into a function:

$$f(x) = g(x) + h(x) \tag{4.15}$$

where g(x) is cost of the shortest path from the starting point to the current node and h(x), the so-called heuristic function, is an estimate of the cost of the shortest path from the current state to the goal. The kind of heuristic is a matter of choice, still it needs to comply with the following three properties:

- Completeness: the algorithm is guaranteed to terminate when dealing with finite graphs having non negative edge weights.
- Admissibility: the heuristic never overestimates the cost of reaching the goal.

$$h(x) \leq h^*(x) \tag{4.16}$$

where h*(x) is defined as the optimal cost to reach a goal from the current node.

- Consistency: the estimate of the algorithm is always less than or equal to the estimated distance from any neighbouring node to the goal, plus the cost of reaching that node.

Time complexity strongly depends on the heuristic and in its worst case (the case in which the search space is unbounded), the number of nodes exploded is exponential in the depth of the solution:

$$d : O(b^d) \tag{4.17}$$

where b is defined as the branching factor. In its best case (the search space is a tree and there exists only one goal) it would develop in a polynomial fashion, provided that the following condition on the heuristic holds:

$$|h(x) - h^*(x)| = O(\log h^*(x)) \tag{4.18}$$

where h* is the optimal heuristic. For this reason, a bounded relaxation is applied: it is possible to speed up the process by considering also approximate shortest paths. This process is bounded by a factor ϵ so that optimality suffers a decrease that is not greater than $(1 + \epsilon)$ times the optimal solution, computed without the hypothesis relaxation. Several possible algorithms exists for ϵ, below is reported as an example the Dynamic Weighting, Pohl [19]:
cost function is defined as

$$f(n) = g(n) + (1 + \epsilon w(n))h(n) \tag{4.19}$$

where w(n) is

$$w(n) = \begin{cases} 1 - \frac{d(n)}{N}, & \text{if } d(n) \leq N \\ 0, & \text{otherwise} \end{cases} \tag{4.20}$$

with d(n) being the depth of the search and N the anticipated length of solution. Below is reported the pseudocode of the A^* algorithm:

It is interesting to note that the algorithm returns either the optimal plan, hence it is an exact algorithm.

Algorithm 4.3 A algorithm

```
Input: A graph G(V,E) with source node start and goal node end
Output Least cost path from start to end
open_list = start
closed_list =
g(start) = 0
h(start) = heuristic_function(start,end)
f(start) = g(start) + h(start)
while open list is not empty do
  m = Node on top of open_list, with least f
  if m == end then
    return
  end if
  remove m from open_list
  add m to closed_list
  for each n in child(m) do
    if n in closed_list then
      continue
    end if
    cost = g(m) + distance(m,n)
    if n in open_list and cost < g(n) then
      remove n from open list as new path is better
    end if
    if n in closed_list and cost < g(n) then
      remove n from closed list
    end if
    if n not in open_list and n not in_closed list then
      add n to open_list
      g(n) = cost
      h(n) = heuristic_function(n, end)
      f(n) = g(n) + h(n)
    end if
  end for
end while
return  failure
```

Figure 4.6: A* initial problem: red point is the starting node, green point is the goal

(a) a (b) b (c) c

Figure 4.7: Shortest path relaxing the admissibility criteria

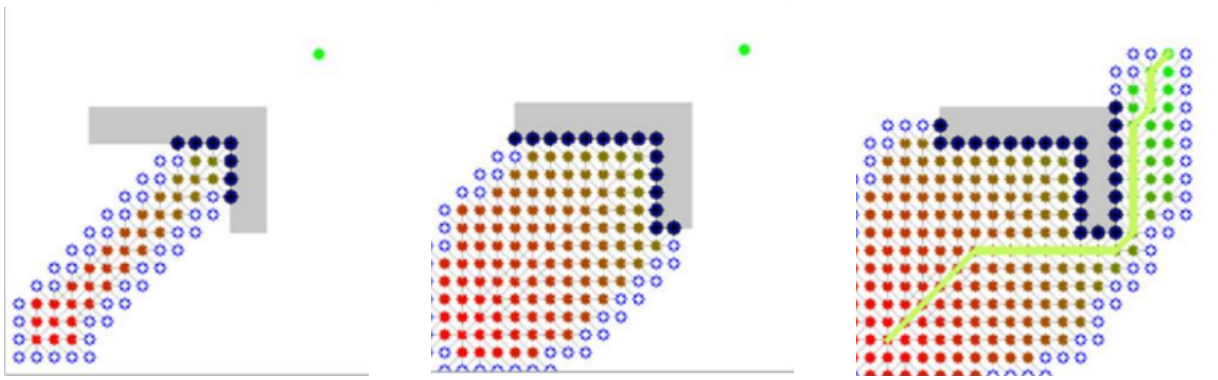

(a) a (b) b (c) c

Figure 4.8: Optimal path obtained using the admissibility criteria.

4.4. Local Planning

A strong assumption on which global planning technique was based is the fact that the space surrounding the robot from its starting point to its goal is almost totally known. Nonetheless, robots moving in every environment must be able to deal with unforeseen changes and adapt to them. For this purpose, a local planner is paired with the global planner: while the latter is responsible of trajectory planning and works at a low frequency rate, the first one deals with trajectory following and obstacle avoidance at a much higher frequency rate. So, local planning is deemed to solve two tasks:

- Ensure path following
- Perform obstacle avoidance for objects that are not tracked in the map

Obstacle Avoidance "Let A be the robot moving in the workspace W, whose configuration space is CS. Let q be a configuration, q_t this configuration in time t, $A(q_t) \in W$ the space occupied by the robot in this configuration. If in the vehicle there is a sensor, which in qt measures a portion of the space $S(q_t) \subset W$ identifying a set of obstacles $O(q_t) \subset W$. Let u be a constant control vector and $u(q_t)$ this control vector applied q_t during time δt. Given $u(q_t)$, the vehicle describes a trajectory
$q_t + \delta_t = f(u, q_t, \delta t)$, with $\delta t \geq 0$. Let Q_t, T be the set of the configuration of the trajectory followed from q_t with $\delta t \in (0, T)$ a given time interval. T > 0 is called the sampling period. Indicating with $q_t target$ a target configuration. Then, in time t_i the robot A is in $q_t i$, where a sensor measurement is obtained $S(q_{ti})$, and thus an obstacle description $O(q_t i)$." Siciliano and Khatib [22] The overall goal of the obstacle avoidance algorithm is to find a trajectory from that brings the robot closer to the goal in a non colliding way:
$A(q_{ti}, T) \cap O(q_t i) = \emptyset$
$f(q_{ti}, q_{target}) \leq F(q_{ti} + T, q_{target})$

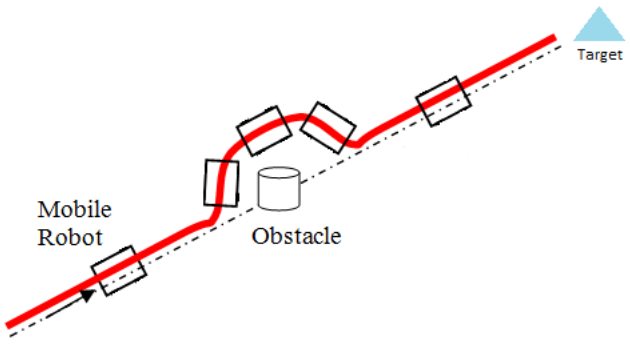

Figure 4.9: Sample of the most simple obstacle avoidance technique

In the following subsections an overview of the most famous local planning method will be provided, in particular:

- Vector Field Histogram
- Curvature Velocity
- Dynamic Window Approach

4.4.1. Vector Field Histograms

Vector Field Histogram was presented in 1991 by Borenstein and Koren [4] and ensured fast obstacle detection and collision avoidance, not requiring the vehicle to stop. It is composed of two steps, where the first one all the possible motions are evaluate and in the second one the best one is traversed.

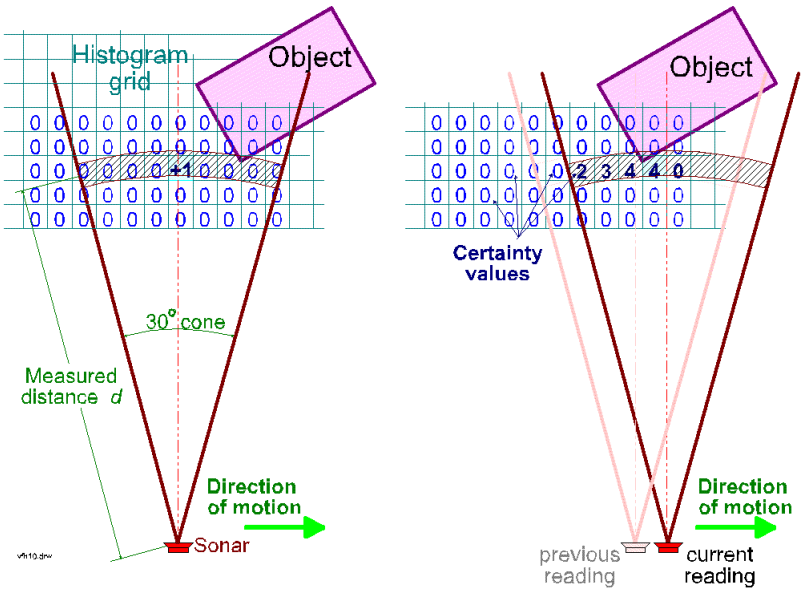

Figure 4.10: Vector Field Histogram

The Vector Field Histogram is based on the concept of virtual force field, a concept that resort somehow to the idea of imaginary forces acting on a robot, Khatib [11]. VFF is composed of:

- A two-dimensional Cartesian histogram grid for obstacle representation, where the grid is composed of cells defined by some coordinate (i,j) and $c_{i,j}$ holds the probability of the occupancy. A probability distribution is created by updating only one cell in the histogram grid for each range reading. More specifically, the function $h^k(q_{ti})$ describes the density of the obstacle, on turn proportional to the probability

of point occupancy P(p) and to distance from the obstacle, that is to say that the more the distance increases, the lower is the density. The function $h^k(q_{ti})$ is defined as:

$$h^k(q_{ti}) = \int_{\Omega_k} P(p)^n \left(1 - \frac{d(q_{ti}, p)}{d_{max}}\right)^m dp \tag{4.21}$$

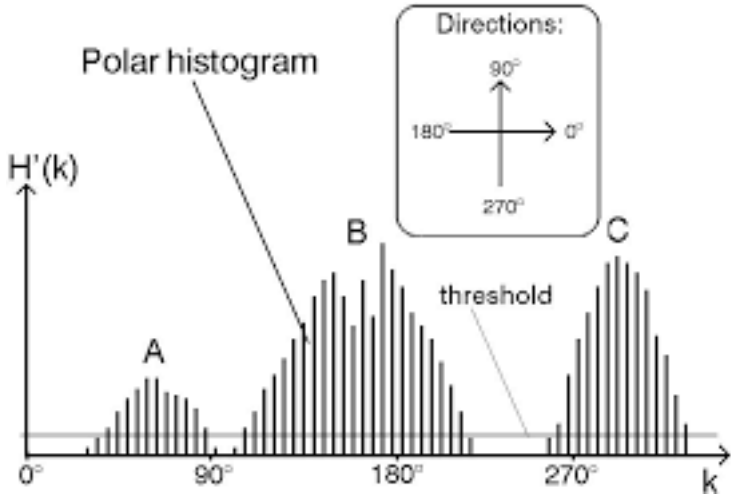

Figure 4.11: Vector Field Histogram

- Application of potential field idea to the histogram grid
- Previous two component are combined in real time enables sensor data to perform obstacle avoidance

All the directions ranged from the sensors are evaluated but only those that fall under the defined threshold are further investigated. A cost function is then established as follows:

$$G = \alpha \times target\_direction + \beta \times wheel\_orientation + \gamma \times previous\_direction \tag{4.22}$$

where α represents the direction of the goal, β the smoothing of the action and γ the previous direction of motion. Every direction, falling under the threshold, is evaluated through the newly defined cost function, that becomes the selection method.

4.4.2. Curvature Velocity Methods

Curvature Velocity Methods were developed by Reid Simmons in 1996. This approach to obstacle avoidance treats the problem as a constrained optimization in the velocity space of the robot, rather than in Cartesian space. The robot is deemed to travel along arcs of circles rather than straight lines, still it cannot turn instantaneously. This method works

by adding constraints to the velocity space, defined as the set of controllable velocities and choosing the point in that space that complies with all the constraints and maximizes an objective function, that balances speed, safety and goal-directedness, Simmons [24].

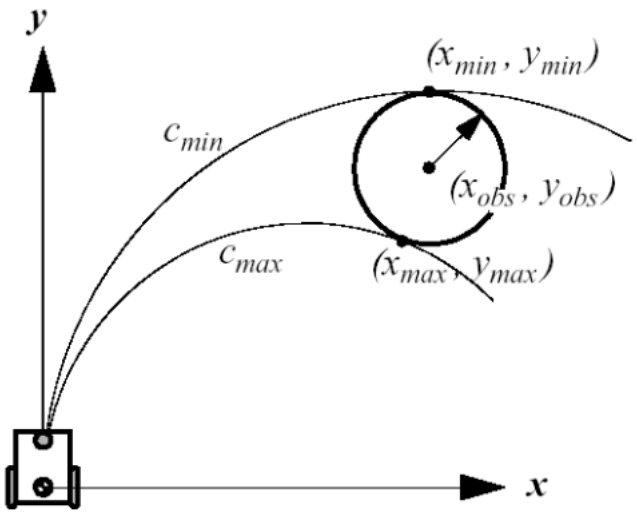

Figure 4.12: Curvature Velocity Methods

Only the interval of curvatures between c_{min} and c_{max} are considered, where the set of considered trajectories is obtained by using the curvatures tangent to obstacles to divide the velocity space into regions of constant distance.

4.4.3. Dynamic Window Approach

The dynamic window approach is an obstacle avoidance technique developed by Dieter Fox, Wolfram Burgard and Sebastian Thrun in 1997. In the DWA approach, the search for commands to control the robot takes place directly in velocity space. Compared to the previously seen method, the robot's dynamics are also integrated, thus further constraining the velocity search space to those that respect the dynamics constraints and are safe with respect to the obstacle. The process can be divided into search space and optimization, Fox et al. [7]. The search space of the possible velocities is reduced in three points:

- Circulare Trajectories: only circular trajectories are considered, determined by pair of (v,w) translational and rotational velocities
- Admissible Velocities: restriction to consider only safe velocities
- Dynamic Window: further restriction that applies to the admissible velocities, selecting only those that can be reached within a short time interval, respecting the constraints on acceleration.

The dynamic windows search space reduces to $V_r = V_s \cap V_a \cap V_d$

Optimization step proposes to maximize the objective function

$$G(v, w) = \sigma(\alpha \times heading(v, w) + \beta \times dist(v, w) + \gamma \times vel(v, w)) \tag{4.23}$$

where *heading* is a measure of progress towards goal location, *dist* is the distance towards the closest obstacle and *vel* is the the foward velocity of the robot.

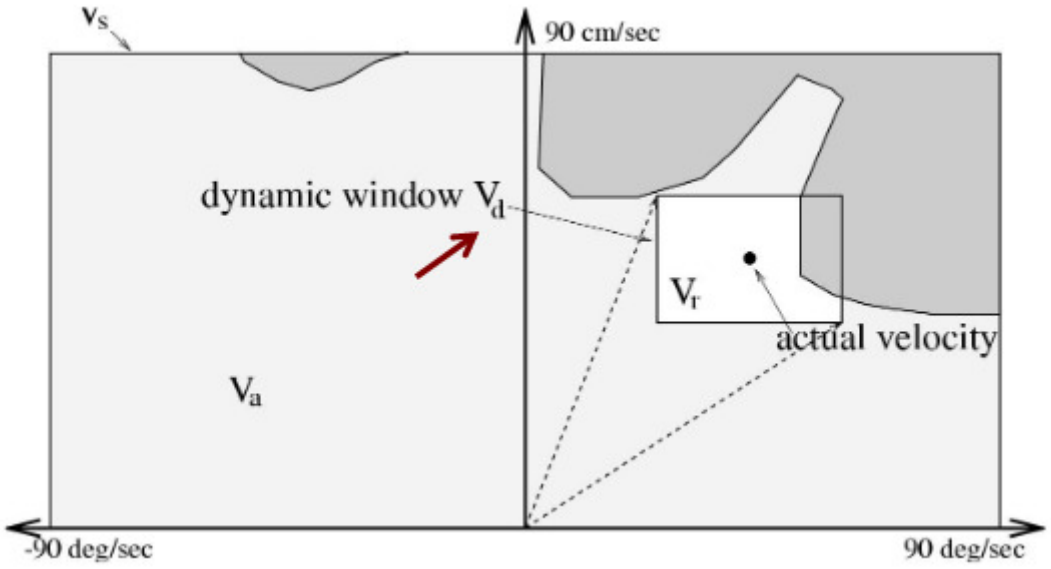

Figure 4.13: Dynamic Window

Algorithm 4.4 DWA algorithm

```
BEGIN DWA(robotpose, robotGoal, robotModel)
desired_V = calculate_V(robotPose,robotGoal)
laserscan = readScanner()
allowable_v = generateWindow(robot_V, robotModel)
allowable_w = generateWindow(robot_W, robotModel)
for each v in allowable_v do
  for for each w in allowable_w do
    dist = find_dist(v,w,laserscan,robotModel)
    breakDist = calculateBreakingDistance(v)
    if (dist > breakDist) then
      heading = hDiff(robotPose,goalPose, v,w)
      clearance = (dist-breakDist)/(dmax - breakDist)
      cost = costFunction(heading,clearance, abs(desired_v − v))
      if (cost > optimal) then
        best_v = v
        best_w = w
        optimal = cost
      end if
    end if
  end for
end for
set robot trajectory to best_v, best_w
```

Contribution

- **Chapter 5: Simulator and Testing Platform**
- **Chapter 6: Pointcloud Filter**

5 | Simulator and Testing Platform

5.1. Introduction

Part of the work carried out at Oversonic Robotics was the development of a simulator and testing platform. The simulator, described in section 5.2, is primarily intended to be a safe and reliable test environment where the new navigation algorithms can be tested. It is not intended to have a 1:1 simulation with the real robot, which is outside the scope of this thesis. As already mentioned, building robots means dealing with both the software and hardware side, the two components are inseparable and one does not exist without the other. Dealing with the hardware part of the robot is a source of danger for people and the environment as software bugs can cause damage. In addition, testing a robot's behaviour in real life, the results of which are unknown, can cause mechanical damage and consequently much time would be lost in repair. Another not inconsiderable motivation lies in the wear and tear of the robot and its components: the batteries, for example, have a predefined life cycle and must be recharged in any case. All these reasons support the development of a simulated environment to test new developments before implementing them on the real robot. The testing module, described in section 5.3, addresses the need to have an indication of navigation performance. This need comes both from within the company, where it is important to evaluate how developments are improving it, and from outside, where the various stakeholders and customers can evaluate the project and understand how they can exploit the technology developed by Oversonic. Not only this, as reported by Dhillon [6], among the many types of tests, two of them are significant:

- Reliability: obtain knowledge of failure occurrence patterns
- Performance: building reliable indicators on performance status

Tests are moreover meant to have the following features:

- Accuracy: whether the test can actually measure what it sets out to measure
- Resolution: how precisely it measures the proposed feature
- Repeatability: how repeatable it is, so that test performed over time are comparable

5.2. Simulator

5.2.1. Introduction

As already mentioned, the development of this simulator meets the practical need to be able to test new navigation algorithms in a safe manner. Given this need, the choice of simulation engine fell on Gazebo. The reasons behind this choice are many: Gazebo provides seamless integration with ROS and Rviz, and allows the working environment to be customised to the maximum, creating its own model of the robot, motors and sensors. On the other hand, this great freedom that is granted requires just as much expertise and an analytical study of the robot model. The approach we decided to follow was to first familiarise ourselves with the creation of three-dimensional models in URDF and XACRO by developing simple robot models and then adding sensors, as to make the model more articulated. Once familiar with the development environment, it was decided to create a model as faithful as possible to the R007 robot, combined with a differential drive base.

5.2.2. 3D Model Creation

The designed robot is made up of the following components:

- a core box, representing the structure of the robot
- two-wheel drive, one on the right and one on the left side
- two caster wheels, one in the front and one in the back. They are completely passive and the provide robot stability
- two Lidars, one place on the front and one on the back of the robot

First of all it is necessary to define the physical dimensions of the robot e.g. base dimensions, wheel parameters. It is also necessary to specify the inertia values for every mass component existing: the core of the robot, the wheels and the caster wheels. A robot can be described as having a number of link components and a number of joint elements that connect the links. The link element describes a stiff body with collision characteristics, visual characteristics (specifying the shape of the object for visualization purposes), and inertia.

The links used in this model were:

- Robot core: base link and dummy link
- Wheels: right and left wheel

- Caster wheels: right and left caster wheel
- Lidar: front and back lidar

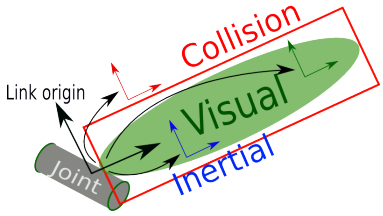

Figure 5.1: Link representation that better explains the concepts of collision and visual

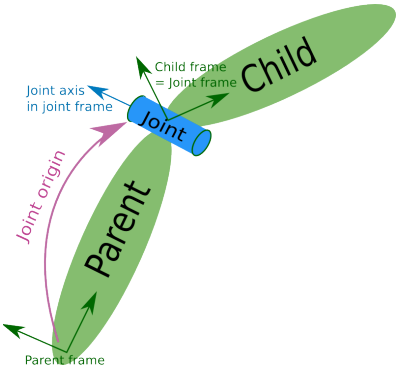

Figure 5.2: Joint visual representation

The joint element sets the joint's safety restrictions and explains the kinematics and dynamics of the joint. There exists several types of joint, but in this specific application continuous joint was used for the casters and wheels, whereas fixed joint for the robot core and Lidar were used. Because it cannot move, a fixed joint is not really a joint: every level of freedom is locked. Continuous hinge joints have no upper or lower limitations and rotate about their axes, in this case particular attention must be paid to the collision parameters: friction has to be properly calibrated in the case of caster wheels, since a wrong friction or slip coefficient impedes the robot to turn properly. Since this simulator is not intended to be a 1:1 with the movements performed by the real robot, still we do not want friction to constrain movements, slip coefficient has been set to 1 whereas friction coefficient to 0. This choice has been made by trial and error, since by modifying those values, the robot could not follow the planner trajectories, leading to continuous drift.

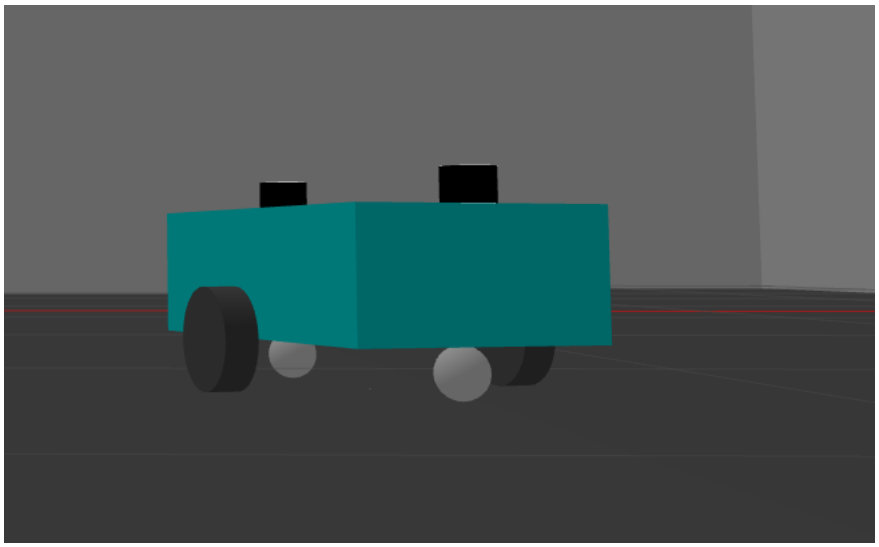

Figure 5.3: Robot model visualization

The complete code that builds the model up can be found at Appendix A.

5.2.3. Gazebo Plugins

The strategy up to this point has been to create the 3D model of the robot, then specify the components and their dimensions, links and joint types. At this point the model is created but is no more than a mesh and cannot be used in navigation. In order to get the robot on track, it is necessary to duly integrate the model with a drive system, which mimics the physical motors, and lidar sensors. Gazebo provides plug-ins that meet this requirement. Two main plug-ins were used within the simulator: the differential_drive_controller for differential driving and the head_hokuyo_controller for lidar. In order to have the differential drive plug in working, a number of parameters must be set to bind it to the created XACRO model and to the already existing navigation stack. In particular, the plug-in needs to know the dimensions of the wheels and the joints to which they are connected, as well as the link of the robot body and the odometry topic. The speed command is acquired directly from the topic /twist_mux/cmd_vel, which is also used in the real robot. It is then necessary to specify the torque to be applied and the update rate. A similar argument must be made for the integration of the lidar sensor plug-in. It is necessary to specify all the topics that are normally used in the real robot to build a bridge between the simulated environment and the navigation stack. In particular, the topics used are /scanHF and /scanHB. It is also appropriate to modify the specifications of the simulated sensor to match those of YDlidar G4. In addition, the plug-in for the d455 camera and the t265 camera can also be imported. The simulated

depth camera can be used for the recognition of tags placed in the virtual environment as well as for pointcloud generation. The simulated tracking camera, on the other hand, is used for visual odometry by replacing the default odometry source parameter of the differential drive with the topic of the tracking camera.

5.2.4. Virtual Environment

The next step was to create a virtual environment where the robot can move and where the navigation algorithms can be tested. The approach used was to replicate the Oversonic Robotics development space. After acquiring the measurements of the real environment with laser metre, the 1:1 scale measurements were transported to the Gazebo environment. Gazebo in fact allows the creation of rooms from scratch, building walls and doors with centimetre-accurate measurements. It also allows the insertion of obstacles and fiducial tags in the space.

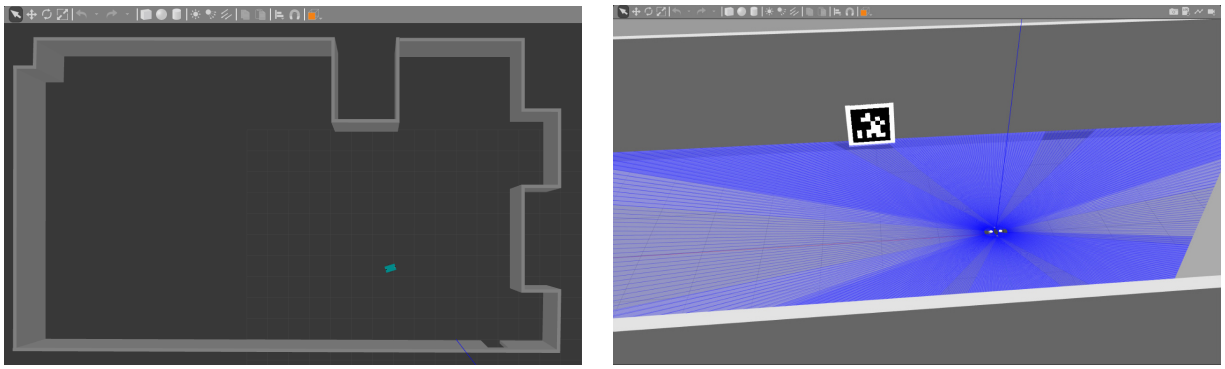

(a) Bird's eye view of the virtual environment (b) Apriltag integration

Figure 5.4: Production room simulated environment

5.2.5. Mapping and Navigating

After constructing the virtual environment, the mapping of the new space is required. A launcher must then be set up to run all the simulation components created. Within the launch file, the newly created simulated world, the robot model with the required plug-ins and an Rviz spawner will be imported. Similar to what happens in the real world, we proceed to move the robot with the joystick and the SLAM toolbox takes care of creating a map. Once the map is obtained and cleared, the robot's navigation module can be tested. In figure 5.5 is reported an example of obstacle avoidance performed by the simulated robot.

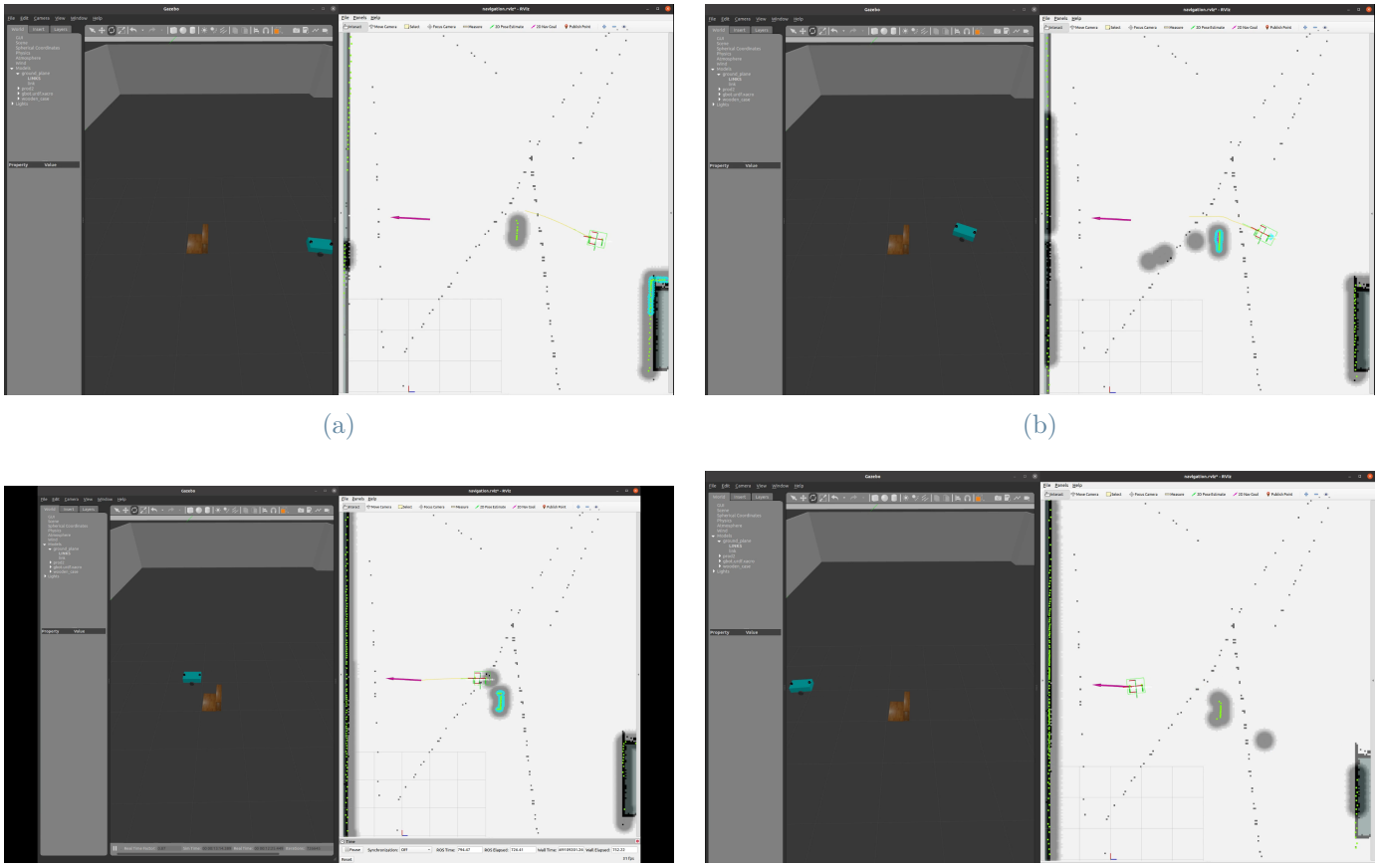

(a) (b)

(c) (d)

Figure 5.5: Simulation of an obstacle avoidance movement

5.3. Testing Module

The test module is designed to be a highly autonomous instrument where the operator only needs to indirectly monitor its progress. To this end, the module was developed in Python, supplementing the original navigation stack with a part dedicated to plotting the route in real time and calculating statistics. Starting from an unknown work are, the steps to be followed are as follows:

1. Build the map of the environment (using SLAM toolbox), clean it from anomalies and load it on Oversonic database

2. Design the path the robot is going to follow during its tests: the path has to respond to specific behaviors we want to test, e.g. relocation via Apriltag, climbing a ramp, navigate close to walls and obstacles. Specify the starting position, a list of way-points and a goal point, building a json file with their coordinates and uploading it

to database

3. Decide robot's configuration and the number of repetitions for the test

Oversonic adopts waypoint logic for its navigation tasks: waypoint navigation is a commonly used approach in mobile robots navigation. When the robot has to perform predefined path (for example in testing framework, as this thesis is) it is convenient to specify some points between its starting and arriving point where the robot has to pass by or near by. In the scope of this thesis, a new waypoint is sent as a goal to the robot when at a distance of less than one metre from the last received waypoint. Clearly, tests are significant only if repeated for a high number of times so that meaningful statistics are set up. Test pattern is thus set up via Oversonic's interface where it is possible to load test configuration:

- Robot: which robot is going to perform the movement
- Map: where the robot will be moving
- Mission: the path it is going to run
- Repetitions: how many times should the mission iterates

Once the configurations are set, the interface lets the test responsible to select the number of repetitions the robot is going to perform.

5.3.1. Performance Measurement Definition

As introduce, tests need to be accurate, resolute and repeatable. For the purpose of performance measurement, the following values of interest are given for each measurement configuration:

- AVG SPEED: average speed over the entire path [m/s]
- FW AVG SPEED: average speed while navigating (its the avg speed from which we exclude on-site rotations) [m/s]
- ROT AVG SPEED: rotational average speed [rad/s]
- NAV DISTANCE: total distance calculated by odometry [m]
- TOP SPEED: top speed recorded [m/s]
- NAV TIME: total time spent [s]
- FW MOVING TIME: moving forward time [s]

- ROTATING TIME: time the robot spends rotating in place [s]
- OBSTACLES: number of obstacles on the path [-]

The Navigation Performance index, also known as NP, is a metrics that returns the goodness of the navigation for a set of measurements. It has been developed to provide a summary indicator of performance at a glance.

$$NP = W * X = \begin{bmatrix} w_1 & w_2 & w_3 & w_4 \end{bmatrix} \begin{bmatrix} x_1 \\ x_2 \\ x_3 \\ x_4 \end{bmatrix} \tag{5.1}$$

The formula is defined by the vector product of the row vector W with column vector X. X gathers four states measurements:

$$x_1 = \frac{NavigatedDistance}{PathDistance} \tag{5.2}$$

$$x_2 = \frac{ForwardAverageSpeed}{RequestedSpeed} \tag{5.3}$$

$$x_3 = \frac{MovingFwTime}{NavigationTime} \tag{5.4}$$

$$x_4 = \texttt{min}(OBSTACLES * 0.25; 1) \tag{5.5}$$

whereas W is a vector that is used to weight the states on the overall performance. The values of the weights have been chosen trying to penalize blocking movements and trying to promote the ones that keeps the robot forward speed high.

$$W = \begin{bmatrix} 25 & 25 & 30 & 20 \end{bmatrix} \tag{5.6}$$

Overall the NP index has the following formulation:

$$NP = \frac{w_1 * x_1 + w_2 * x_2 + w_3 * x_3 + w_4 * x_4}{w_1 + w_2 + w_3 + w_4} = \frac{15 * x_1 + 30 * x_2 + 25 * x_3 + 30 * x_4}{100} \tag{5.7}$$

5.3.2. Code Explanation

The testing module is based on a callback structure. A ROS node called 'measures' is initialised and subscribed to three topics: goal_status, cmd_vel_mux_out and odom. We begin by explaining the concept of goal_status. In fact, it is necessary to know what status the robot is in in order to distinguish the various phases and obtain reliable statistics. The built in class of Oversonic `goal_status` arbitrates the management of statuses in a tree structure and decides to send the global status to the mission service. A global status, called goal_status arbitrates two sub-states: move_base_flex and motion_status Move_base_flex is provided by move_base package and handles the statuses as:

- Pending = 0
- Active = 1
- Preempted = 2
- Succeeded = 3
- Aborted = 4
- Rejected = 5
- Preempting = 6
- Recalling = 7
- Recalled = 8
- Lost = 9

The motion_status is still an enumerate and takes the same states as the move_base. Arbitrage checks the statuses and the last updated one, if coincident, is sent to the mission service. For proper test handling, a subclass, called rel_movement_status, was then implemented. The states are defined as:

- Not started = 0
- Navigating = 1
- Rotating = 2
- Reversing = 3
- Stuck = 4

This class monitors the robot's movements and understands if it is advancing, rotating or if it is stuck. The status provided does not enter into the arbitration mentioned above, but is simply an aid to the collection of measurement data and does not communicate with the mission service. Only when both statuses are completed does the global status send the mission completion signal to the mission service via an MQTT message dispatcher. Cmd_vel_mux is a topic that exchanges messages regarding the velocity command: a multiplexer for command velocity inputs. Arbitrates incoming cmd_vel messages from several topics, allowing one topic at a time to command the robot, based on priorities. It also dislocates current allowed topic if no messages are received after a configured timeout. All topics, together with their priority and timeout are configured through a YAML file. In our case, the two topics entering the mux are: the autonomous navigation cmd_vel and the joystick steering cmd_vel. The yaml file has been configured to give priority to joystick control. The last topic is odom and simply provides the message regarding odometry. At this point, the three topics are used within a callback where each time they communicate a message, data is collected and used to calculate statistics. The programme handles the logic through a while loop that remains active until ROS is active or, more selectively, until the goal status is succeeded. Specifically the module not only provides overall statistics but also compute performance intra waypoints. This feature was introduced in order to get a better glance of where the robot suffered from issues or where navigation speed decreased. This was possible by managing goal status in a different manner: waypoints are sent to the robot via a MQTT message and a new waypoint is sent to the robot only when it arrives around a waypoint with customisable accuracy. So every time a new waypoint is delivered to the system, statistics are computed and saved. When eventually the robot reaches the goal, the overall statistics for the lap are computed and saved into a separated xls file. The files are saved in subfolder of the navigation module, called `Datasheets`, where two files are initialized (if not already existing):

- `Waypoints.xls`: statistics of intra waypoints performance are saved. Three relevant metrics are chosen (Distance travelled, Time spent and Average Speed) and each data row corresponds to an intra waypoint measurement. After reaching the goal, the programm splits the set of measurements by inserting an end row.
- `Measurements.xls`: relevant metrics per lap are saved in each row, where column performance indicators are as defined in subsection 5.3.1.

The full description of the python code and for a detailed breakdown of how statistics are computed refer to Appendix B.

5.3.3. Test Case

The route created involves a path of approximately 25 m that involved passing through a 1 m wide doorway. The plot in figure 5.6 is obtained through the designed plotter. The automatic relocation algorithm using fiducial tags of known position on the map is also tested. There are no fixed or moving obstacles other than those already mapped in order to take a snapshot of the current status and robustness of navigation under 'stable' conditions

Figure 5.6: Map visualization: theoretical path required. Total distance: 25.0 m

Below are defined the waypoints and the final goal. The assumption is that the starting point, also known as waypoint 0, coincides with the goal. This ensures test to iterate from itself in a loop of laps.

Waypoint Coordinate	x [m]	y [m]
WP1	2.1	6.3
WP2	4.2	5.7
WP3	4.2	3.1
WP4	3.9	-2.2
WP5	1.9	-2.5
WP6	-0.2	-2.4
WP7	0.0	1
WP8	1.2	3.4
GOAL	0.5	6.6

Table 5.1: Waypoints and Goal coordinates

Settings	Robot: R012	
τ [-]	5	
max. acc [m/s^2]	0.9	at speed = 0.6 [m/s]
	1.0	at speed = 0.7 [m/s]
	1.05	at speed = 0.8 [m/s]
slip [-]	0.9	if speed <[0.8 m/s]
	0.8	if speed >= [0.8 m/s]

Table 5.2: Robot Configuration

5.3.4. Experimental Data and Results

Tests were carried out at 3 different desired speeds (0.6, 0.7 and 0.8 m/s) in order to assess how the statistics varied as the required speed changed.

Test Requested Speed at 0.6 m/s

	Avg Speed [m/s]	Fw Avg Speed [m/s]	Rot avg speed [rad/s]	Nav Dist [m]	Top Speed [m/s]	Nav Time [s]	Moving Fw Time [s]	Rotating Time [s]
Requested Speed = 0.6 [m/s]								
AVG	0,48	0,54	0,73	25,00	0,63	52,73	41,04	6,31
MIN	0,39	0,52	0,49	24,69	0,62	49,89	38,90	4,52
MAX	0,50	0,55	0,82	25,57	0,63	64,69	43,84	14,91
VAR	0,0015	0,0001	0,0121	0,0883	0,0000	28,0762	2,4016	14,4604

Table 5.3: Statistics at 0.6 m/s

Observing the data some useful insights can be extracted: the ratio total average speed to requested speed is equal to 79 %, the ratio forward average speed to requested speed is equal to 91%. The performance index suggests a NP value of 71 %. States measurements are evaluated as $x_1 = 0.998$, $x_2 = 0.907$, $x_3 = 0.778$ and $x_4 = 0$, since no obstacle was present.

Test Requested Speed at 0.7 m/s

Requested speed is increased by 16.7 %. The ratio total average speed to requested speed is increades up to 82 %, the ratio forward average speed to requested speed is steady at 91%. The performance index suggests a NP value of 73 % as in the first case. States measurements are evaluated as $x_1 = 1.01$, $x_2 = 0.914$, $x_3 = 0.82$ and $x_4 = 0$, since no obstacle was present. Increasing the speed leads to an increase in all of the performance states.

	Avg Speed [m/s]	Fw Avg Speed [m/s]	Rot avg speed [rad/s]	Nav Dist [m]	Top Speed [m/s]	Nav Time [s]	Moving Fw Time [s]	Rotating Time [s]
Requested Speed = 0.7 [m/s]								
AVG	0,57	0,64	0,82	25,29	0,73	44,01	36,10	3,96
MIN	0,56	0,63	0,70	25,11	0,72	43,64	34,20	3,11
MAX	0,58	0,65	0,90	25,42	0,74	44,59	38,59	4,82
VAR	0,000062	0,000067	0,004414	0,017557	0,000067	0,091824	1,954462	0,287495

Table 5.4: Statistics at 0.7 m/s

Test Requested Speed at 0.8 m/s

Requested speed is increased by 14.3 %. The ratio total average speed to requested speed decreases to 80 %, the ratio forward average speed to requested speed is steady at 91%. The performance index suggests a NP value of 73 % as in the first case. States measurements are evaluated as $x_1 = 1.02$, $x_2 = 0.914$, $x_3 = 0.738$ and $x_4 = 0$, since no

obstacle was present. Increasing the speed does not lead to an increase in the performance states in this case, in particular state x_3 diminishes by - 11.08 %.

	Avg Speed [m/s]	Fw Avg Speed [m/s]	Rot avg speed [rad/s]	Nav Dist [m]	Top Speed [m/s]	Nav Time [s]	Moving Fw Time [s]	Rotating Time [s]
Requested Speed = 0.8 [m/s]								
AVG	0,64	0,73	0,84	25,57	0,83	39,93	29,48	3,92
MIN	0,60	0,72	0,73	25,35	0,82	38,59	28,31	2,90
MAX	0,66	0,75	0,94	26,00	0,84	41,99	32,00	5,93
VAR	0,000433	0,000081	0,004781	0,063281	0,000048	1,482262	1,608357	1,089214

Table 5.5: Statistics at 0.8 m/s

Comments What can be extracted from the metrics is that the optimal speed for the robot, in its current state, is 0.7 m/s. In table 5.6 an overall comparison can be appreciated.

	Avg Speed [m/s]	Fw Avg Speed [m/s]	Rot avg speed [rad/s]	Nav Dist [m]	Top Speed [m/s]	Nav Time [s]	Moving Fw Time [s]	Rotating Time [s]
Requested Speed = 0.6 [m/s]								
AVG	0,48	0,54	0,73	25,00	0,63	52,73	41,04	6,31
MIN	0,39	0,52	0,49	24,69	0,62	49,89	38,90	4,52
MAX	0,50	0,55	0,82	25,57	0,63	64,69	43,84	14,91
VAR	0,0015	0,0001	0,0121	0,0883	0,0000	28,0762	2,4016	14,4604
Requested Speed = 0.7 [m/s]								
AVG	0,57	0,64	0,82	25,29	0,73	44,01	36,10	3,96
MIN	0,56	0,63	0,70	25,11	0,72	43,64	34,20	3,11
MAX	0,58	0,65	0,90	25,42	0,74	44,59	38,59	4,82
VAR	0,000062	0,000067	0,004414	0,017557	0,000067	0,091824	1,954462	0,287495
Requested Speed = 0.8 [m/s]								
AVG	0,64	0,73	0,84	25,57	0,83	39,93	29,48	3,92
MIN	0,60	0,72	0,73	25,35	0,82	38,59	28,31	2,90
MAX	0,66	0,75	0,94	26,00	0,84	41,99	32,00	5,93
VAR	0,000433	0,000081	0,004781	0,063281	0,000048	1,482262	1,608357	1,089214

Table 5.6: Overall comparison of the statistics

Encountered problems and possible solutions

During the tests, some issues were noted:

- **Tracking Camera**: to achieve an acceptable accuracy, the odometry of the T265 camera was calibrated in a first step. By varying these values, the data obtained vary accordingly. A contingent problem is that of the vibrations of the camera support: the oscillations cause too high values to be neglected. In this case, the values were filtered through a saturation filter.
- **Depth camera**: occasionally the camera sees ghost shadows. This issue is critical since when seeing an obstacle that does not clear, robot enters the recovery mode behaviour: this is a particular set of robot movements developed to let the robot escape from a stuck situation. Mainly, the robots tries to navigate backwards, recomputing global and local costmap. If obstacle does not clear or the path planner can't make it to the goal, the robot tries and rotate on place, recomputing again the costmap. In the event that even this attempt does not solve the problem, there are two scenarios: either the operator moves the robot with the joystick to a point where it is able to restart, or the robot reports an error and the mission is aborted. This is crucial since resorting to recovery behaviour mode leads to a huge loss of time and decreases the overall navigation performance. A system has already been implemented to clean up the map at a predetermined frequency in order to solve the problem of obstacle shadowing, still this do not resolve the problem at the origin. An attempt to solve the problem upstream is proposed in chapter 6.
- **Apriltag localization**: only works correctly when the robot is static. It usually happens that the robot arrives at the tag rotating and as soon as it is localised it tends to consistently correct the position but not the angle: it is planned to insert position control logic (to be corrected only if inaccurate) and to stop the robot if localisation is necessary (only when the robot is stationary can the position be re-initialised)
- **Crash test**: caused by wheel climbing up the side of the ramp. It is assumed that motor current peaks will be checked so that dangerous situations can be recognised in advance. Autonomous navigation can be stopped at any time, so that in case of dangerous situation the user can take control of the robot and command it with a joystick.
- **Internet connection**: the responsiveness of the path planner to the various waypoints depends on the Internet connection. If internet lags, waypoints cannot be

received and thus robots does not know where to go next. In order to solve this problem, an offline waypoint system has been implemented.

- **Navigating through a doorway**: there is rarely any difficulty in crossing the doorway. In tests where this occurred, the robot overcame the problem through recovery behaviour.

5.3.5. Path Real Time Plot

In order to accompany the testing module and to give the user visual support, a small plotting module was developed. The task of this programme is to extrapolate the chosen map and waypoint coordinates from the database. A map is initialised in which the waypoints, identified by a number, and the goal are arranged. The linear path between the different waypoints is then plotted and on this the Euclidean distance between them is calculated. The minimum length that the path will have is then obtained, so as to have a reference with respect to the distance that the robot will travel in each lap. When the robot starts to move, two red and blue indicators, representing the amcl_pose and beacon_pose respectively, mark and keep track of the robot's movement on the map. This provides a tool that plots the robot's path in real time. At the end of each lap, i.e. when the robot reaches the goal, the programme saves the image and re-initalises the plot. All this was achieved using the pyplot package, which allows real-time animation. The position data of the robot was extrapolated instead from the respective topics `amcl_pose` and `beacon_pose`.

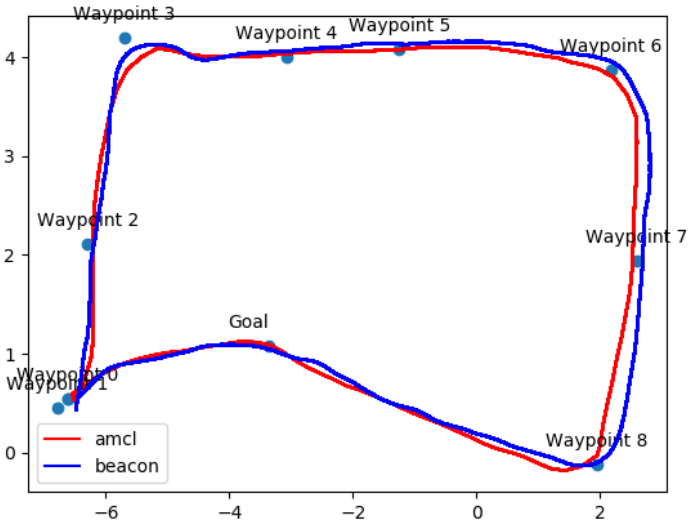

Figure 5.7: Real time plot from beacon and AMCL pose

However, the tool showed some shortcomings in robustness. The problem is mainly caused by the discontinuous signal the beacons send: it is sufficient for the mobile transmitter, placed on the robot, to have its reception field shielded for the modem to stop receiving signals on position tracking. The ultrasounds are in fact completely shielded when the robot and hedgehog are behind a column or physical object relative to the position of the modem transmitter. This is certainly critical with regard to the position plot, which is however an accessory and not a fundamental of testing, but even more so in the case of wanting to calculate the statistics between beacon and amcl pose.

5.3.6. Current Measure

Another addition that was made to the testing module concerns the measurement of currents during navigation. It is indeed important to have an estimate of the current peaks that occur, the hypothetical and actual consumption of the robot. For this purpose, therefore, a programme was created which subscribes to the topic motor_current in a callback and saves all data relating to the left and right motor. This is easily implementable due to the fact that the current message arrives in the form of a multi-array where at positions 0 and 1 are the current data for the left and right motor respectively. It is then possible by dividing by a factor of 10 to obtain the current values directly in ampere. From this data it was straightforward to calculate the data of the absorbed currents in A*h and consequently, by adding them up, estimate the absorption for 1 hour and 8 hours of use.

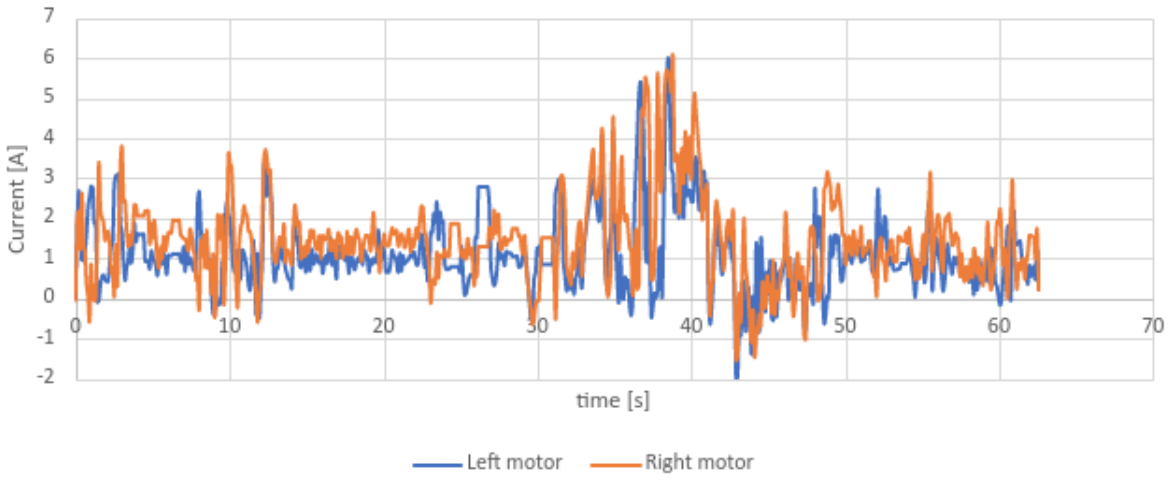

Figure 5.8: Left and Right Motor Current plot

In figure 5.8, the plot of motor current is shown. These data were collected by driving the robot around a path that included the climbing and descending of a ramp. This particular path was a case of interest since an estimate of the battery consumption when

dealing with ramps was needed. The peak of current values indeed correspond to the robot climbing the ramp. In the tables below are reported the computed estimate for a period of 1 and 8 hours.

Hypotetical Consumption	**[Wh]**	**[Ah]**
1 hours	124,0	2,6
8 hours	991,7	20,7

Table 5.7: Energy Consumption

Total Time [s]	62,6
Avg. Absorption [Ah/s]	0,001
Avg. Consumption [Wh/s]	0,034

Table 5.8: Average Absorption and Consumption

The full description of the Python code can be found in Appendix B.

6 | Pointcloud Filter

6.1. Introduction

As introduced in chapter 3, point cloud is a data structure used to represent a collection of multi-dimensional points and is commonly used to represent three-dimensional data. In a 3D point cloud, the points usually represent the X, Y, and Z geometric coordinates of an underlying sampled surface. When color information is present, the point cloud becomes 4D. Point clouds can be acquired from hardware sensors such as stereo cameras, 3D scanners, or time-of-flight cameras, or generated from a computer program synthetically, Rusu and Cousins [21]. In the scope of this thesis, Realsense camera D455 was used in order to perform point cloud generation that was in turn used to generate the occupancy grid of the space around the robot. In figure 6.1 are reported the features of D455 camera.

Sensor Technology	Global Shutter
Ideal Range	from 0.6 m to 6 m
Depth	Technology: Stereoscopic Field of View: 87° x 58° Output Resolution: up to 1280 × 720 Accuracy: <0.02 m at 4 m Frame rate: up to 90 fps
RGB	Technology: Global Shutter Field of View: 90°×65° Output Resolution: up to 1280×800 Sensor Resolution: 1 MP Frame rate: up to 30 fps

Table 6.1: Highlighted camera's specifications.

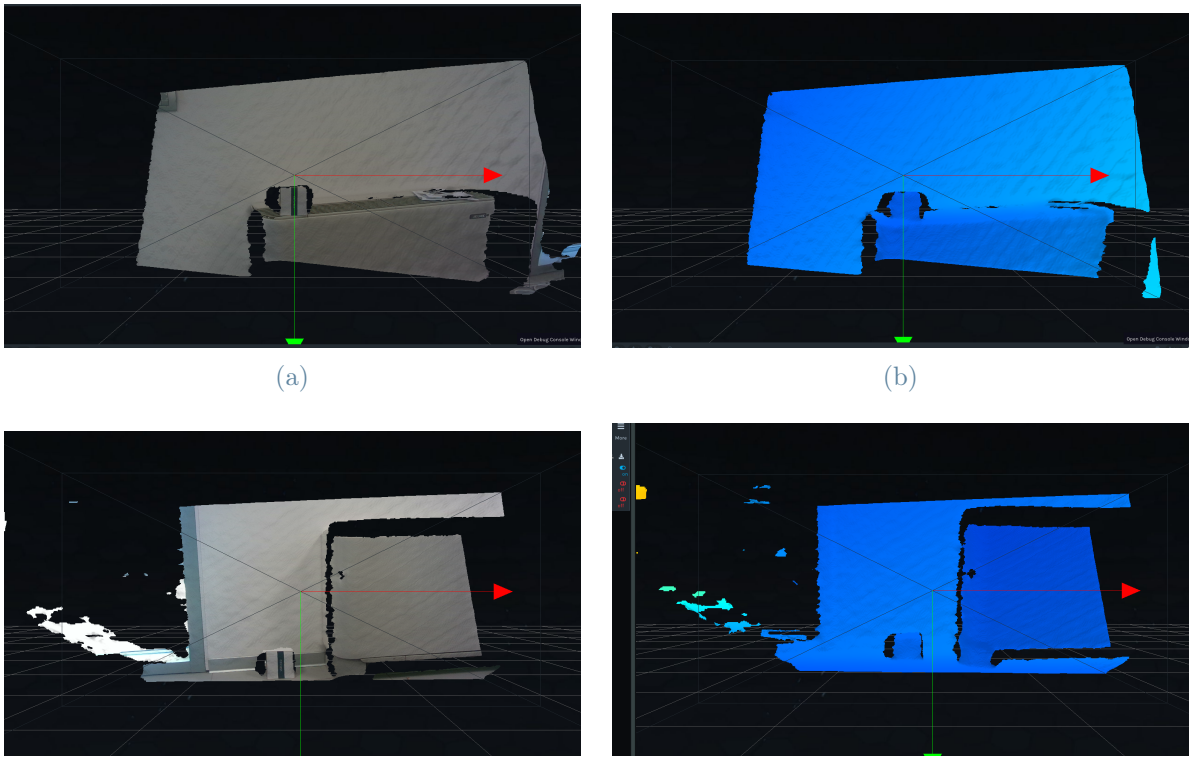

(a) (b)

(c) (d)

Figure 6.1: Pointcloud and RGB-D image visualization from Realsense SDK, taken from D455 camera

The sensor transmits the pointcloud data that are interpreted by ROS in a dedicated format. The PointCloud2 object is an implementation of the `sensormsgs/PointCloud2` message type in ROS. The object contains meta-information about the message and the point cloud data. To access the actual data, use readXYZ to get the point coordinates and readRGB to get the color information, if available. For the pointcloud use in ROS and visualization in RViz environment, two ROS nodes were set up:

- read: reads a point cloud from the camera sensor, publishing it as `sensor_msgs/PointCloud2` message. This message contains a collection of N-dimensional points. The data may be in one dimension, so unordered, or in two dimensions, like images data are stored.
- write: subscribes to the topic `sensor_msgs/PointCloud2`

In order to manage pointcloud data, PCL library was adopted. The Point Cloud Library (PCL) is a standalone, large scale, open project for 2D/3D image and point cloud processing, that provides advanced methods for pointcloud data management and API integration. PCL makes us if a slightly different data class, pcl::PointCloud. This is the

core point cloud class, though having a similar structure to that used in ROS, this enabling a straightforward conversion from PointCloud2 to PCL and viceversa. The motivation for this data class to exist stays in the fact that it enables nodes to work with individual data point as objects rather than with their raw data.

6.2. Problem Explanation

Part of the work at Oversonic Robotics involved testing the state of navigation, as seen in the previous chapter, in order to draw up useful reports both for internal benchmarking and to provide to customers. During these tests, it was realised that, in certain particular indoor and/or outdoor environment conditions, the robot perceived phantom obstacles, which did not exist in reality. This is critical as the objective for the robot's navigation is to perform the programmed path optimally and in the shortest possible time. It is therefore clear that if the local planner encounters these phantom obstacles, a great deal of time is lost and the robot travels a greater distance, also resulting in greater energy consumption. It was therefore decided to devote time to identifying and solving this problem. The conditions that encountered particular problems are:

- Reflective surfaces
- Tiled floor with highly repetitive patterns

In figure 6.6, we can appreciate how the reflective zones of figure a are interpeted as dark areas in figure b, where it is shown RViz GUI.

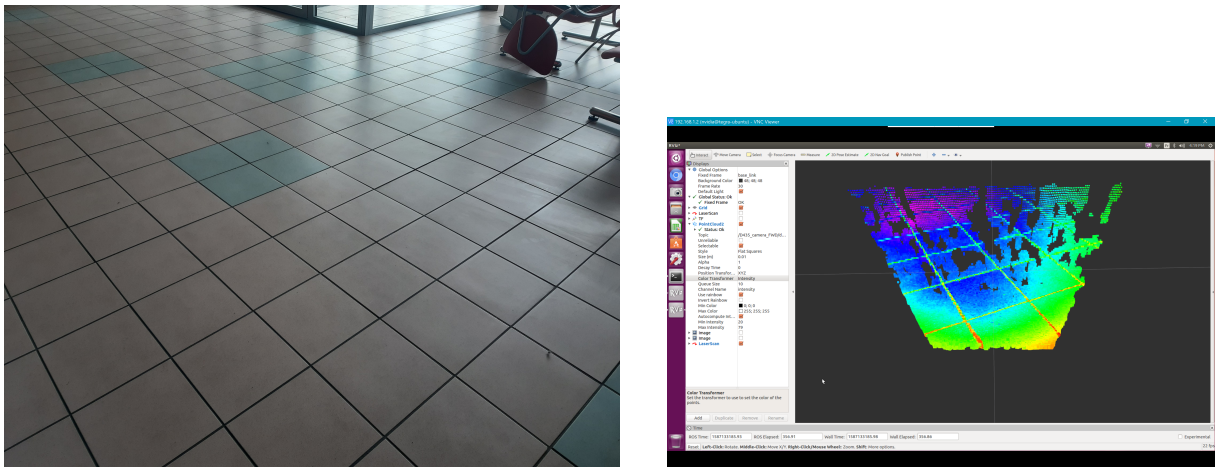

(a) a (b) b

Figure 6.2: Visualization of the reflection issue experimented at Oversonic's office tiled floor

After careful research, it was discovered that many users of the intel realsense chambers were experiencing this problem but no solution was provided by Intel. With the Intel RealSense D400 series of stereo depth cameras, depth is derived primarily from solving the correspondence problem between the simultaneously captured left and right video images, determining the disparity for each pixel (i.e. shift between object points in left vs right images), and calculating the depth map from disparity and triangulation. The Depth RMS error that defines the depth noise for a localized plane fit to depth values can be defined as:

$$DepthRMSerror(mm) = \frac{Distance(mm)^2 \times Subpixel}{focallength(pixels) \times Baseline(mm)} \tag{6.1}$$

Below is reported the findings for D455 RMS error:

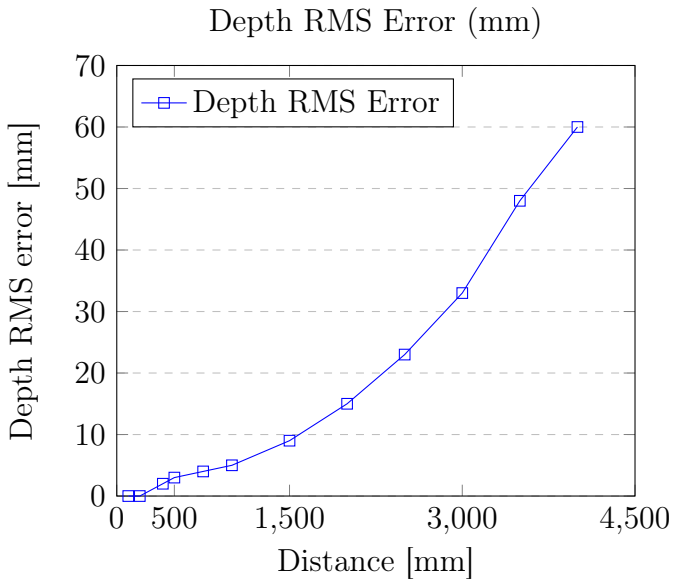

The curve is obtained usind D455 with HFOV=90 deg, Xres=1280, baseline=50 mm and subpixel=0.08. Initially, it was decided to try applying a polarising film to the outer lens of the camera. In figure a polarizer is used to reduce the glare of sunlight reflecting off a window by only passing P-polarized light. Polarizers indeed can be used to selectively attenuate different components of light in order to enhance human vision and photography. The motivation for the use of optical filters comes from Fresnel equations: by properly adopting the filter angulation at Brewster angle, all reflected S-light is polarized, so that all reflections are cancelled. Fresnel divided light into S- and P- polarization states, where S has the electric field normal to the plane of incidence and P has the electric field co planar with it. Glare can lead to local saturation of portions of the image and false depth can result from objects partially reflected from the surface. Glare-induced saturation is

usually associated with bright light sources such as sunlight or light bulbs. Reflection-related false depth typically occurs with textured objects reflected on shiny surfaces with little texture

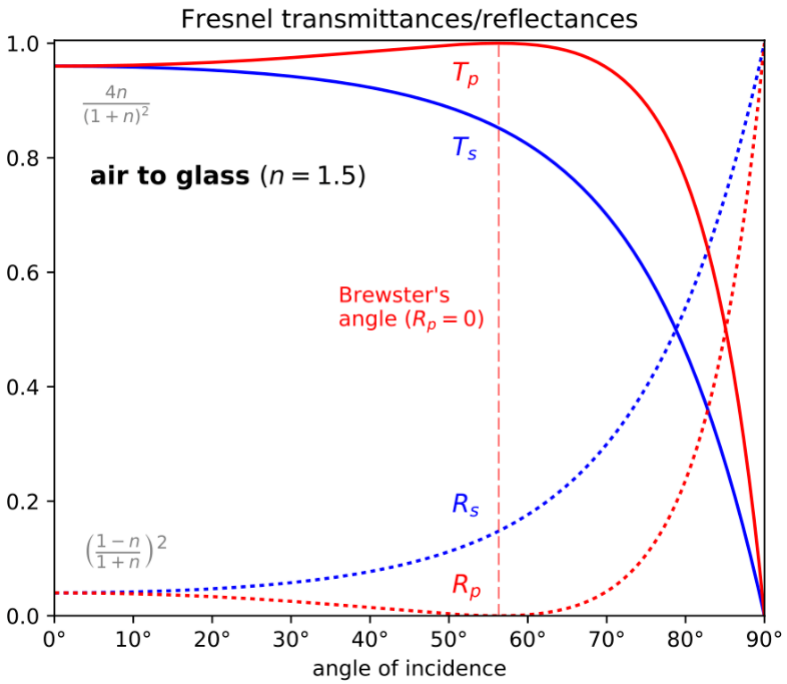

Figure 6.3: Fresnel transmittances/reflectances

Polarizers work well in condition of natural sunlight, as in figure 6.4, but in our working environment the optical filter showd no improvement on detecting ghost obstacles.

Figure 6.4: On the right there is the image taken from D400 RealSense camera, on the left there is the image taken after applying the physical filter on the lens.

In fact, even after applying the optical filter, the robot kept visualizing glare in form of

black spaces, misleading obstacle detection. In order to test the difference in performance with the application of the polarising film, a test identical to that already presented in Chapter 5 was used. In section 6.4, navigation metrics before and after film application can be appreciated.

6.3. Proposed Solution

Since the attempted solution by application of an optical filter led to only marginal improvements, it was decided to resort to a post-processing solution. Intel RealSense SDK provides some buil-in methods to perform filtering, in particular:

- Decimation: reduce resolution of depth frame
- Disparity: transformation between depth and disparity domains
- Spatial: edge-preserving smoothing
- Temporal: filter depth data by looking into previous frames

Promising results were achieved by applying these filters to saved file of pointcloud data, but this approach did not allow to perform real time filtering, so it was left for an online post-processing solution. For this purpose, as already mentioned, the PCL library was used. This library provides methods for filtering pointcloud data. The approach was to treat ghost reflections as a mass of data too dense to be analysed and a statistical outlier removal filter was tried. In fact, the idea behind it is to remove noisy measurements from the pointcloud, as these scattered outliers corrupt the results. The solution therefore proposes statistical analysis around each point neighborhood: for every point compute the distance from the point itself to all of its neighbors. A similar approach was proposed by Ning et al. [17]: The sparse pointcloud P is defined by N points such that $P = p_1, p_2, p_3, ..., p_N$ whereas the k nearest neighbor points of a point p_i are defined as $KNN(p_i)$, a set of k points such that $Q = q_1, q_2, q_3, ..., q_k$. The algorithm removes points that are considered outliers based on geometric information.

The average geometric distance of a point p_i from its neighbors is defined as:

$$d_i = 1/k \sum_{j=1}^{k} dist(p_i, q_j) \tag{6.2}$$

where dist(x,y) is a function that returns euclidean distance between two points. By assuming that the resulted distribution is Gaussian with a mean and a standard deviation, we can derive μ_d the overall mean distance and σ_d, the standard deviation of distances.

Hence, by tuning α, the so-called standard deviation multiplier, we can define a threshold $T = \mu_d + \alpha\sigma_d$. Every point in the cloud, whose its kNN distance falls out of the interval defined by T, are directly discarded. Tuning of α parameter was performed by trial and error. Below is reported the resulting algorithm, algorithm 6.1:

Algorithm 6.1 Statistical Outlier Removal: pure KNN approach

```
Set k
Set α
for P_i in input_data do
    Locate kNN to point P_i
    Compute d_i
end for
Compute μ_d
Compute σ_d
Compute T = μ_d + α σ_d
if d_i > T then
    Trim point P_i from the pointcloud
end if
```

The problem can be solved from another point of view that is by analyzing clusters of isolated pointcloud data, Ning et al. [16]. Local density function, $LD(p_i$ of p_i is introduced as:

$$LD(p_i) = \frac{1}{k} \sum_{q_j \in KNN(p_i)} exp(\frac{-dist(p_i, q_j)}{d_i} \tag{6.3}$$

The probability that a point belongs to outlier can be defined as $prob(p_i) = 1 - LD(p_i)$, where $prob(p_i) = 1 - LD(p_i)$ and it ranges between 0 and 1, so that a higher value means a higher probability for the point to be outlier. The point p_i is retained if it falls under some predefined threshold, like T in previous approach, so $prob(p_i) < \delta$. The threshold is not intended to be universal, rather its value depends on its case of application.

Algorithm 6.2 Statistical Outlier Removal: local density approach

```
Set k
Set α
for P_i in input_data do
    Locate kNN to point P_i
    Compute LD(P_i)
    Evaluate probability prob(p_i)
end for
sort prob(p_i) in ascending order
if prob(p_i) > δ then
    Trim point P_i from the pointcloud
end if
```

In figure 6.5 the overall process flow is described.

Figure 6.5: Overall process block scheme

As initially stated, the goal of this filter is to perform online processing of point cloud. In our specific case, we want to take input data, perform the data transformations and then output both the filtered and original data, so that the user can choose which to keep. Input data are transmitted from and to the ROStopic `/d400_lb/depth/color/points` through the subrscribe and publish paradigm. In order to work on the data with the PCL methods, it is necessary to transform the message structure from `PointCloud2` to PCL format and transform back to `PointCloud2` after the filtering has occured. A crucial point for this approach is computing time, given the fact that we want the filter to process the data at real time. It was necessary to provide an indication of the time required for the filter to elaborate the data, in order to understand its practical feasibility. Initially, pre processing was made on the data and the filter was dealing with the entire amount of point cloud information at the same time. This led to an extremely high computing time

(0.5 s) that is unacceptable for obstacle detection, in fact this brought to a further drop of navigation performance. It was thought that the problem was caused by a too strong filtering action, so we tried to decrease further the threshold. This was a misconcept, since after a careful analysis it was discovered that the delay was introduced by the conversion of data format from PointCLoud2 to PCL format. The only solution left at this point was to try and pre-process the data using a decimation filter, in order to feed the code with the least required amount of data. Decimation filter is has been designed by Intel RealSense to effectively reduce the depth scene complexity. The filter run on kernel sizes [2x2] to [8x8] pixels. For patches sized 2 and 3 the median depth value is selected. For larger kernels, 4-8 pixels, the mean depth is used due to performance considerations, Dev [5]. In order to understand which configuration worked better inside the computational time constraint, several tests were conducted. In table 6.2 average results are reported, key indicators are:

- Converting Time represents the 2-way cost of converting data: from PointCloud2 to PCL and from PCL back to PointCloud2
- Processing Time represents the computational cost of performing the statistical outlier removal on the input cloud

Configuration	**Converting Time [s]**	**Processing Time [s]**	**Total Time [s]**
Pre-filter: none Filter: K=50	0.42	0.13	0.55
Pre-filter: none Filter: K=9	0.25	0.09	0.34
Pre-filter: decimation Filter: K= 50	0.07	0.03	0.10
Pre-filter: decimation Filter: K= 9	0.04	0.01	0.05

Table 6.2: Comparison of average computational times implied by different filter - prefilter configurations

This data was collected and analysed by running the code on a camera detached from the robot. Once the configurations to be tested had been chosen, the physical robot was moved on. The idea was to define an initial benchmark, obtained from chapter 5, and to collect useful data to compare the same metrics with the chosen configurations. The aim was to analytically assess whether and to what extent the various configurations could

improve the management of phantom reflections and the performance of navigation in general.

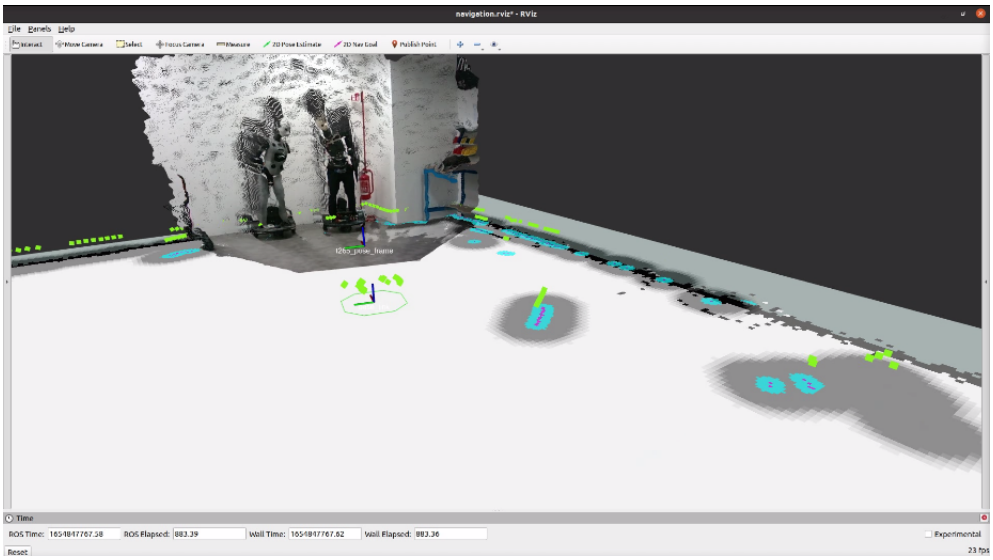

(a) a

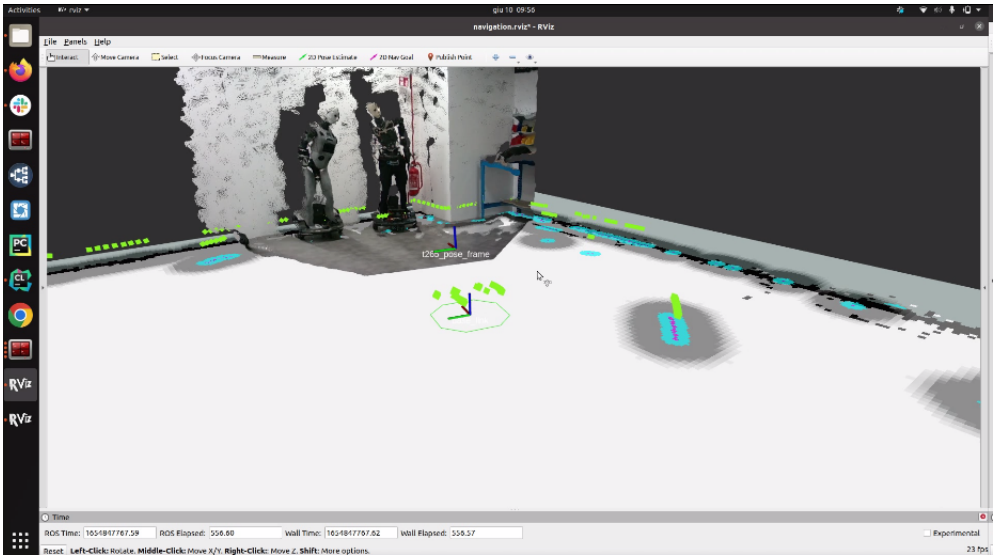

(b) b

Figure 6.6: Pre and post filtering comparison

.

Overall, the designed process flow resulted as reported in algorithm: 6.3:

Algorithm 6.3 Postprocesser

Set magnitude of decimation filter
Set k
Set α
Subscribe pointcloudtopic
Input_data: pointcloud topic
for P_i in input_data **do**
  Convert from PointCloud2 to PCL::cloud
  Locate kNN to point P_i
  Compute d_i
end for
Compute μ_d
Compute σ_d
Compute $T = \mu_d + \alpha\sigma_d$
if $d_i >$ T **then**
  Trim point P_i from cloud
end if
Output_data = cloud
for P_i in cloud **do**
  Convert from PCL to PointCloud2
end for
publish pointcloud topic and pointcloud_filtered topic

The complete code written in C++ can be found in appendix B.

6.4. Experimental Results

In order to assess what impact the introduction of the pointcloud filter had, the N002 robot was subjected to a test session on the same path used in the chapter 5. Of the various configurations tested, only the most significant are presented below for conciseness. All configurations were tested five times, under the same lighting conditions, in order to ensure the comparability of the results. Stuck time is introduced.

6.4.1. Starting configuration: no pointcloud filter, no prefilter

Nav Avg Speed [m/s]	Mov Fw Avg Speed [m/s]	Rot Avg Speed [m/s]	Nav Time [s]	Rotating Time [s]	Stuck Time [s]
0.44	0.5	0.61	56.79	6.35	0.23
0.46	0.52	0.63	53.69	4.44	0.33
0.46	0.51	0.64	53.79	3.94	0.12
0.45	0.51	0.63	54.14	3.94	0.41
0.46	0.51	0.66	53.99	3.9	0.11

Table 6.3: Measurements with original set up

6.4.2. Pointcloud filter with K=9, no prefilter

Nav Avg Speed [m/s]	Mov Fw Avg Speed [m/s]	Rot Avg Speed [m/s]	Nav Time [s]	Rotating Time [s]	Stuck Time [s]
0.45	0.5	0.65	55	4.52	0.11
0.45	0.5	0.63	54.6	4.5	0.1
0.46	0.51	0.65	53.69	4.81	0.01
0.46	0.51	0.64	54.09	5.61	0.19
0.46	0.52	0.61	52.89	5.35	0.11

Table 6.4: Pointcloud filter k=9, no prefilter

6.4.3. Pointcloud filter with K=9, decimation prefilter

Nav Avg Speed [m/s]	Mov Fw Avg Speed [m/s]	Rot Avg Speed [m/s]	Nav Time [s]	Rotating Time [s]	Stuck Time [s]
0.46	0.52	0.61	53.49	5.13	0.033
0.46	0.52	0.59	53.19	5.5	0.035
0.47	0.53	0.64	52.39	4.92	0.052
0.46	0.52	0.65	53.6	5.52	0.081
0.46	0.52	0.6	52.8	4.92	0.061

Table 6.5: Pointcloud filter K=9, decimation filter

6.5. Comments

In reporting the measurements from these tests, the focus was on the statistics on the average linear and angular velocities of navigation and the times the robot remained in the predefined states. In order to assess the improvements made, particular attention should be paid to the Navigation and Stuck time values. These in fact come into play when the robot recognises obstacles to be overcome and consequently, increase in value. It can be seen that the initial configuration presents average navigation and stuck times of 54.48 s and 0.24 s respectively. By inserting the pointcloud filter with a filter power dictated by K=9, the values drop to 54.05 s and 0.104 s. Since the computation time still proved to be high, i.e. one tenth of a second, it was decided to try prefiltering the incoming data to the filter in order to lighten the amount of data to be analysed. The results were promising, leading to a browsing time of 53.1 s and a stuck time of 0.052 s, at the cost of an average computation time of 0.05 s. These differences may seem marginal, but when transported in the context of the use of many working hours, they take on a non-negligible importance. The inclusion of the pointcloud filter has also resulted in a more continuous navigation that allows the robot to reach its objectives in less time and avoiding discontinuities in movements that can accelerate wear and tear in the long run.

7 | Conclusions and future developments

In the first part of this work, a simulator was developed from scratch to test new navigation algorithms. This made it possible to test the new custom recovery behaviour, for example, first in the simulated environment and once the goodness of the development was seen, it was implemented in the real robot. Consequently, a testing platform was developed that provides a comprehensive overview of performance measurements, motor current data and a robot trajectory visualiser. During testing, a problem was observed with the depth camera, which recognised reflections on the floor as obstacles. A real time filter was then implemented to decrease the density of the pointcloud data. Thanks to this, it was possible to solve the problem of phantom obstacles by decreasing the stuck time, in a computational time that does not affect the result. The simulator could be subject to further improvements in the future: one possible route that could be taken would be to break free from gazebo plug-ins, for example by modelling the differential drive on a par with that used in the real robot. Furthermore, in order to make the simulated model completely mirror the real one, another possibility that could be pursued would certainly be to analytically model friction and wheel slip. As far as the pointcloud filter is concerned, other possible solutions can be tested: there are several filters for manipulating the point cloud, the results of which have yet to be tested.

Bibliography

[1] On hedgehogs and marvelous minds: A new technology for point data collection?

[2] I. Asimov. *Runaround*. 1942.

[3] R. K. Base. URL `https://roboticsknowledgebase.com/wiki/state-estimation/adaptive-monte-carlo-localization/`.

[4] J. Borenstein and Y. Koren. The vector field histogram - fast obstacle avoidance for mobile robots. *Robotics and Automation, IEEE Transactions on*, 7:278 – 288, 07 1991. doi: 10.1109/70.88137.

[5] I. R. Dev. Decimation filter. URL `https://dev.intelrealsense.com/docs/post-processing-filters`.

[6] B. S. Dhillon. *Robot Testing and Information Related to Robots*, pages 210–225. Springer New York, New York, NY, 1991. ISBN 978-1-4612-3148-6. doi: 10.1007/978-1-4612-3148-6_12. URL `https://doi.org/10.1007/978-1-4612-3148-6_12`.

[7] D. Fox, W. Burgard, and S. Thrun. The dynamic window approach to collision avoidance. *IEEE Robotics Automation Magazine*, 4(1):23–33, 1997. doi: 10.1109/100.580977.

[8] M. Herzog. Dikstra's algorithm. URL `https://www-m9.ma.tum.de/graph-algorithms/spp-dijkstra`.

[9] Intel. Robust visual-inertial tracking from a camera that knows where it's going. URL `https://www.intelrealsense.com/visual-inertial-tracking-case-study/`.

[10] E. T. Jonasson, L. Ramos Pinto, and A. Vale. Comparison of three key remote sensing technologies for mobile robot localization in nuclear facilities. *Fusion Engineering and Design*, 172:112691, 2021. ISSN 0920-3796. doi: https://doi.org/10.1016/j.fusengdes.2021.112691. URL `https://www.sciencedirect.com/science/article/pii/S0920379621004671`.

[11] O. Khatib. Real-time obstacle avoidance for manipulators and mobile robots. In

Proceedings. 1985 IEEE International Conference on Robotics and Automation, volume 2, pages 500–505, 1985. doi: 10.1109/ROBOT.1985.1087247.

[12] P. Lima, D. Nardi, G. Kraetzschmar, J. Berghofer, M. Matteucci, and G. Buchanan. Rockin innovation through robot competitions [competitions]. *Robotics Automation Magazine, IEEE*, 21:8–12, 06 2014. doi: 10.1109/MRA.2014.2314015.

[13] S. Macenski and I. Jambrecic. Slam toolbox: Slam for the dynamic world. *Journal of Open Source Software*, 6(61):2783, 2021. doi: 10.21105/joss.02783. URL `https://doi.org/10.21105/joss.02783`.

[14] M. Montemerlo, S. Thrun, D. Koller, and B. Wegbreit. Fastslam: A factored solution to the simultaneous localization and mapping problem. 11 2002.

[15] MQTT.org. Mqtt.org. URL `https://mqtt.org/`.

[16] X. Ning, F. Li, G. Tian, and Y. Wang. An efficient outlier removal method for scattered point cloud data. *PLOS ONE*, 13(8):1–22, 08 2018. doi: 10.1371/journal.pone.0201280. URL `https://doi.org/10.1371/journal.pone.0201280`.

[17] X. Ning, F. Li, G. Tian, and Y. Wang. An efficient outlier removal method for scattered point cloud data. *PLoS ONE*, 13, 2018.

[18] E. Olson. AprilTag: A robust and flexible visual fiducial system. In *Proceedings of the IEEE International Conference on Robotics and Automation (ICRA)*, pages 3400–3407. IEEE, May 2011.

[19] I. Pohl. The avoidance of (relative) catastrophe, heuristic competence, genuine dynamic weighting and computational issues in heuristic problem solving. In *Proceedings of the 3rd International Joint Conference on Artificial Intelligence*, IJCAI'73, page 12–17, San Francisco, CA, USA, 1973. Morgan Kaufmann Publishers Inc.

[20] Repubblica, 2022. URL `https://www.repstatic.it/content/contenthub/img/2022/05/24/114226177-5cef6076-990d-4f67-b7ae-03d1cc734ee3.jpg?webp`.

[21] R. B. Rusu and S. Cousins. 3D is here: Point Cloud Library (PCL). In *IEEE International Conference on Robotics and Automation (ICRA)*, Shanghai, China, May 9-13 2011.

[22] B. Siciliano and O. Khatib, editors. *Springer Handbook of Robotics*. Springer, Berlin, Heidelberg, 2008. ISBN 978-3-540-23957-4. URL `http://dx.doi.org/10.1007/978-3-540-30301-5`.

[23] B. Siciliano and O. Khatib. *Humanoid Robots: Historical Perspective, Overview*

and Scope, pages 1–6. Springer Netherlands, Dordrecht, 2020. ISBN 978-94-007-7194-9. doi: 10.1007/978-94-007-7194-9_64-1. URL https://doi.org/10.1007/978-94-007-7194-9_64-1.

[24] R. Simmons. The curvature-velocity method for local obstacle avoidance. In *Proceedings of IEEE International Conference on Robotics and Automation*, volume 4, pages 3375–3382 vol.4, 1996. doi: 10.1109/ROBOT.1996.511023.

[25] S. Thrun, M. Montemerlo, D. Koller, B. Wegbreit, J. Nieto, and E. Nebot. Fastslam: An efficient solution to the simultaneous localization and mapping problem with unknown data. *Journal of Machine Learning Research*, 4, 05 2004.

[26] S. Thrun, W. Burgard, and D. Fox. *Probabilistic Robotics*. Intelligent Robotics and Autonomous Agents series. MIT Press, 2005. ISBN 9780262201629. URL https://books.google.ch/books?id=k_yOQgAACAAJ.

[27] R. Wiki. Concepts, . URL http://wiki.ros.org/ROS/Concepts.

[28] R. Wiki. Manifest, . URL http://wiki.ros.org/Manifest.

[29] R. Wiki. Metapackages, . URL http://wiki.ros.org/Metapackages.

[30] R. Wiki. msg, . URL http://wiki.ros.org/msg.

[31] R. Wiki. Nodes, . URL http://wiki.ros.org/Nodes.

[32] R. Wiki. Packages, . URL http://wiki.ros.org/Packages.

[33] R. Wiki. Parameter server, . URL http://wiki.ros.org/Parameter20Server.

[34] R. Wiki. Services, . URL http://wiki.ros.org/Services.

[35] R. Wiki. srv, . URL http://wiki.ros.org/srv.

[36] R. Wiki. Topics, . URL http://wiki.ros.org/Topics.

A | Appendix A

A.1. XACRO code of the model

```
<?xml version="1.0"?>
<robot xmlns:xacro="http://www.ros.org/wiki/xacro" name="navbot">

  <xacro:property name="base_width" value="0.3"/>
  <xacro:property name="base_length" value="0.5"/>
  <xacro:property name="base_height" value="0.15"/>
  <xacro:property name="wheel_radius" value="0.06"/>
  <xacro:property name="wheel_width" value="0.04"/>
  <xacro:property name="wheel_separation" value="0.38"/>
  <xacro:property name="wheel_joint_offset" value="0.02"/>
  <xacro:property name="caster_wheel_radius" value="0.03"/>
  <xacro:property name="caster_wheel_joint_offset" value="0.2"/>
  <xacro:property name="laser_radius" value="0.03"/>
  <xacro:property name="laser_len" value="0.04"/>

  <xacro:include filename="$(find nav-sim)/urdf/calculations.xacro" />
  <xacro:include filename="$(find nav-sim)/urdf/materials.xacro" />


<!-- BASE LINK -->
  <link name="base_link">
    <visual>
      <origin xyz="0 0 0" rpy="0 0 0"/>
        <geometry>
          <box size="0.001 0.001 0.001" />
        </geometry>
    </visual>
  </link>

  <link name="chassis">
    <xacro:box_inertia m="10" w="${base_width}" h="${base_height}" d="${base_length}"/>
    <collision>
      <origin xyz="0 0 ${base_height/2}" rpy="0 0 0"/>
      <geometry>
        <box size="${base_length} ${base_width} ${base_height}"/>
      </geometry>
    </collision>
    <visual>
      <origin xyz="0 0 ${base_height/2}" rpy="0 0 0"/>
```

```
      <geometry>
        <box size="${base_length} ${base_width} ${base_height}"/>
      </geometry>
      <material name="water"/>
    </visual>
  </link>

  <joint name="base_link_joint" type="fixed">
    <origin xyz="0 0 ${wheel_radius}" rpy="0 0 0" />
    <parent link="base_link"/>
    <child link="chassis"/>
  </joint>


<!--WHEELS -->

  <xacro:macro name="wheel" params="prefix reflect">
    <link name="${prefix}_wheel">
      <xacro:cylinder_inertia m="2" r="${wheel_radius}" h="0.005"/>
<!--       TODO: add rotation in inertia-->
      <visual>
        <origin xyz="0 0 0" rpy="${pi/2} 0 0"/>
        <geometry>
          <cylinder radius="${wheel_radius}" length="${wheel_width}"/>
        </geometry>
        <material name="orange"/>

      </visual>
      <collision>
        <origin xyz="0 0 0" rpy="${pi/2} 0 0"/>
        <geometry>
          <cylinder radius="${wheel_radius}" length="${wheel_width}"/>
        </geometry>
    <joint name="${prefix}_wheel_joint" type="continuous">
      <origin xyz="0 ${((wheel_separation/2))*reflect} 0"
      rpy="0 0 0"/>
      <parent link="chassis"/>
      <child link="${prefix}_wheel"/>
      <axis xyz="0 1 0"/>
    </joint>
  </xacro:macro>

  <xacro:wheel prefix="left" reflect="1"/>
  <xacro:wheel prefix="right" reflect="-1"/>


<!-- CASTER WHEELS -->

  <xacro:macro name="caster_wheel" params="prefix reflect">
    <link name="${prefix}_caster_wheel">
      <xacro:sphere_inertia m="1" r="${caster_wheel_radius}"/>
      <visual>
        <origin xyz="0 0 0" rpy="0 0 0"/>
```

```
      <geometry>
        <sphere radius="${caster_wheel_radius}"/>
      </geometry>
      <material name="black"/>
    </visual>
    <collision>
      <origin xyz="0 0 0" rpy="0 0 0"/>
      <geometry>
        <sphere radius="${caster_wheel_radius}"/>
      </geometry>
      <surface>
      <friction>
        <ode>
          <mu>0</mu>
          <mu2>0</mu2>
          <slip1>1.0</slip1>
          <slip2>1.0</slip2>
        </ode>
      </friction>
    </surface>
    </collision>
  </link>

  <joint name="${prefix}_caster_wheel_joint" type="continuous">
    <axis xyz="1 1 1"/>
    <parent link="chassis"/>
    <child link="${prefix}_caster_wheel"/>
    <origin xyz="${reflect*caster_wheel_joint_offset} 0 ${-wheel_radius+caster_wheel_radius}"
    rpy="0 0 0"/>
  </joint>
</xacro:macro>

<xacro:caster_wheel prefix="front" reflect="1"/>
<xacro:caster_wheel prefix="back" reflect="-1"/>


<!--LASERS-->
<xacro:macro name="laser" params="suffix reflect">
  <link name="laser_frame_${suffix}">
    <visual>
      <origin xyz="0 0 0" rpy="0 0 0"/>
      <mass value="1" />
      <geometry>
        <cylinder radius="${laser_radius}" length="${laser_len}"/>
      </geometry>
    </visual>
    <collision>
      <origin xyz="0 0 0" rpy="0 0 0"/>
      <geometry>
        <cylinder radius="${laser_radius}" length="${laser_len}"/>
      </geometry>
    </collision>
    <xacro:cylinder_inertia m="1" r="${laser_radius}" h="${laser_len}"/>
```

```
    </link>
    <joint name="laser_joint_${suffix}" type="fixed">
      <origin xyz="${reflect*(base_length/2-laser_radius)} 0 ${base_height+laser_len/2}" rpy="0 0 0"/>
      <parent link="chassis" />
      <child link="laser_frame_${suffix}" />
    </joint>
  </xacro:macro>

  <xacro:laser suffix="HF" reflect="1"/>
  <xacro:laser suffix="HB" reflect="-1"/>


<!--  <xacro:include filename="$(find nav-sim)/urdf/_d435.urdf.xacro" />-->
<!--  <sensor_d435 parent="chassis">-->
<!--    <origin xyz="0 0 0" rpy="0 0 0"/>-->
<!--  </sensor_d435>-->

  <xacro:include filename="$(find nav-sim)/urdf/navbot_gazebo_plugins.gazebo.xacro"/>

</robot>
```

B | Appendix B

B.1. Testing Module

```
#!/usr/bin/env python
from math import sqrt
from pathlib import Path
import rospy
from geometry_msgs.msg import Twist
from nav_msgs.msg import Odometry
from openpyxl import Workbook
from openpyxl import load_workbook
from cros.topics import ROSTopics
rospy.init_node("measures")
rospy.loginfo("Started measuring ...")
RATE = 10  # Hz
rate = rospy.Rate(RATE)
# filename = "../measurement.xlsx"  # save in isc_slam
rounding = 2
filename = Path.home() / 'MEASURES/measurement.xlsx'

def cb_status(msg):
    global goal_status
    status_array = msg.status_list
    try:
        goal_status = status_array[len(status_array) - 1].status
    except:
        # rospy.loginfo("status not received yet")
        goal_status = 0

def cb_cmd_vel(msg):
    global cmd_vel, cmd_vel_received
    cmd_vel = msg
    cmd_vel_received = True


def cb_odom(msg):
    global odom, top_speed
    odom = msg
    top_speed = max(top_speed, msg.twist.twist.linear.x)


movement = 0  # [0: not started, 1: navigating, 2: rotating,\\
```

```
3: backwards, 4:stuck]

cmd_vel = Twist()
odom = Odometry()
goal_status = 0
nav_time = 0
nav_dist = 0
nav_speed_integral = 0
nav_avg_speed = 0
top_speed = 0

cmd_vel_received = False
fw_time = 0
fw_speed_integral = 0
fw_avg_speed = 0

rot_time = 0
rot_speed_integral = 0
rot_avg_speed = 0

back_time = 0
stuck_time = 0

stopped = True
rospy.Subscriber(ROSTopics.GOAL_STATUS.name, ROSTopics.GOAL_STATUS.data_class,
cb_status)
rospy.Subscriber(ROSTopics.CMD_VEL_MUX_OUT.name, ROSTopics.CMD_VEL_MUX_OUT.data_class,
cb_cmd_vel)
rospy.Subscriber(ROSTopics.T265_ODOM.name, ROSTopics.T265_ODOM.data_class, cb_odom)


while not rospy.is_shutdown():
    last_time = rospy.Time.now()
    last_pos = [odom.pose.pose.position.x, odom.pose.pose.position.y]
    while not goal_status == 0:  # if navigation started at least once
        dt = (rospy.Time.now() - last_time).to_sec()
        ds = sqrt((odom.pose.pose.position.x - last_pos[0]) ** 2 +
        +(odom.pose.pose.position.y - last_pos[1]) ** 2)
        last_time = rospy.Time.now()
        last_pos = [odom.pose.pose.position.x, odom.pose.pose.position.y]
        # print("cycle - ", last_time.to_sec())

        if goal_status == 1:  # if in navigation
            if stopped:
                stopped = False

            # GENERAL IF MOVE BASE IS NAVIGATING
            nav_time += dt
            nav_dist += ds
            nav_speed_integral += odom.twist.twist.linear.x * dt
            nav_avg_speed = nav_speed_integral / nav_time

            # IF ROBOT IS REQUESTING FORWARD MOVEMENT
```

```
        if cmd_vel_received and cmd_vel.linear.x > 0.05:
        # if received cmd_vel requesting of going forward
            if movement != 1:
                rospy.loginfo("Navigating...")
                movement = 1
            fw_time += dt
            fw_speed_integral += odom.twist.twist.linear.x * dt
            fw_avg_speed = fw_speed_integral / fw_time

        # IF ROBOT IS ROTATING ON PLACE
        if cmd_vel_received and abs(cmd_vel.linear.x) < 0.05 and abs(
                cmd_vel.angular.z) >= 0.1:
                # if received cmd_vel requesting of going forward
            if movement != 2:
                rospy.loginfo("Rotating on place...")
                movement = 2
            rot_time += dt
            rot_speed_integral += abs(odom.twist.twist.angular.z) * dt
            rot_avg_speed = rot_speed_integral / rot_time

        # IF ROBOT IS MOVING BACKWARDS
        if cmd_vel_received and odom.twist.twist.linear.x < - 0.05:
        # measuring time while going backwards
            if movement != 3:
                rospy.loginfo("Going backwards...")
                movement = 3
            back_time += dt

        # STUCK ON PLACE
        # if cmd_vel_received and abs(odom.twist.twist.linear.x) < 0.05
        and abs(odom.twist.twist.angular.z) < 0.05:
        if cmd_vel_received and abs(odom.twist.twist.linear.x) < 0.05
        and abs(odom.twist.twist.angular.z) < 0.1 \
                and cmd_vel.angular.z < 0.1:
            if movement != 4:
                rospy.loginfo("Stuck...")
                movement = 4
            stuck_time += dt

        cmd_vel_received = False  # resetting to False to check if cmd_vel is still
        received in the next loop

    elif goal_status == 3 and not stopped:  # stopped to print results just once
        rospy.loginfo("Robot arrived to goal")
        # PRINT SPEEDS
        print("nav_avg_speed: ", round(nav_avg_speed, 2),

              " | mov_fw_avg_speed:", round(fw_avg_speed, 2),
              " | rot_avg_speed:", round(rot_avg_speed, 2),
              " | nav_dist:", round(nav_dist, 2),
              " | top_speed:", round(top_speed, 2))
        # PRINT TIMES
        print("nav_time:      ", round(nav_time, 2),
```

```
                " | moving_fw_time:  ", round(fw_time, 2),
                " | rotating_time:", round(rot_time, 2),
                " | back_time:", round(back_time, 2),
                " | stuck_time:", round(stuck_time, 2))
            List = [nav_avg_speed, fw_avg_speed, rot_avg_speed, nav_dist,
                    top_speed, nav_time, fw_time, rot_time, back_time, stuck_time]
            List = [round(num, rounding) for num in List]

            try:
                wb = load_workbook(filename)
                ws = wb.worksheets[0]  # select first worksheet
            except FileNotFoundError:
                headers_row = ['Speed req.', 'tot_avg_speed', 'fw_avg_speed',
                               'rot_avg_speed', 'nav_dist', 'top_speed',
                               'nav_time', 'moving_fw_time', 'rotating_time',
                               'back_time', 'stuck_time']
                wb = Workbook()
                ws = wb.active
                ws.append(headers_row)
            ws.append(List)
            wb.save(filename)

            stopped = True
        rate.sleep()
```

B.2. Current Measure

```
def _cb_motor_current(self, msg: Float32MultiArray):
    t_now = time.time()
    delta_t = t_now - self._last_time_motor
    # get values of current of the wheels, divide by 10 for hardware reason
    self._l_current = msg.data[0] / 10
    self._r_current = msg.data[1] / 10
    # evaluate the absorbed current in [A*h] for each wheel (Ampere * hour)
    self._r_consume = self._r_current * delta_t / 3600
    self._l_consume = self._l_current * delta_t / 3600
    if not self.differential_drive:
        self._rl_current = msg.data[2] / 10
        self._rr_current = msg.data[3] / 10
    else:
        self._rl_current = 0
        self._rr_current = 0
    self._rl_consume = self._rl_current * delta_t / 3600
    self._rr_consume = self._rr_current * delta_t / 3600
    # evaluate the sum of the absorbed current of each wheel
    total_consume = self._r_consume + self._l_consume + self._rl_consume + self._rr_consume
    self._e_abs += total_consume
    self._last_time_motor = t_now
```

B.3. Postprocesser

```
// First, include ros library
#include <ros/ros.h>
// Include then pcl library required
   #include <pcl_conversions/pcl_conversions.h>
   #include <pcl/point_cloud.h>
   #include <pcl/point_types.h>
   #include <pcl/filters/voxel_grid.h>
   #include <pcl/filters/statistical_outlier_removal.h>
   #include <pcl/filters/statistical_outlier_removal.h>
   #include <pcl/io/pcd_io.h>

// Include PointCloud2 message
#include <sensor_msgs/PointCloud2.h>

// Topics (corrected, needs to be checked)
static const std::string IMAGE_TOPIC = "/d400_lb/depth/color/points";
static const std::string PUBLISH_TOPIC = "/pointcloudfiltered";

using namespace std::chrono;

// ROS Publisher
ros::Publisher pub;
int i;

void cloud_cb(const sensor_msgs::PointCloud2ConstPtr& cloud_msg)
{

    auto start = high_resolution_clock::now();
    // Container for original & filtered data
    pcl::PCLPointCloud2* cloud = new pcl::PCLPointCloud2;
    pcl::PCLPointCloud2ConstPtr cloudPtr(cloud);
    pcl::PCLPointCloud2 cloud_filtered;

    // Convert to PCL data type
    pcl_conversions::toPCL(*cloud_msg, *cloud);
    //filtering with StatisticalOutlierRemoval
    pcl::StatisticalOutlierRemoval<pcl::PCLPointCloud2> sor;
    sor.setInputCloud(cloudPtr);
    sor.setMeanK(9);
    sor.setStddevMulThresh(1.0);
    sor.filter(cloud_filtered);
    // Convert to ROS data type
    sensor_msgs::PointCloud2 output;
    pcl_conversions::moveFromPCL(cloud_filtered, output);
    // Publish the data
    pub.publish (output);
    auto stop = high_resolution_clock::now();
    auto duration = duration_cast<microseconds>(stop - start);
    std::cout << duration.count() << std::endl;
}
int main (int argc, char** argv)
```

```
{
    // Initialize the ROS Node ""
    ros::init (argc, argv, "subscriber_filter_republisher");
    ros::NodeHandle nh;
    // Create a ROS Subscriber to IMAGE_TOPIC with a queue_size of 1 and a callback
    function to cloud_cb
    ros::Subscriber sub = nh.subscribe(IMAGE_TOPIC, 1, cloud_cb);
    // Create a ROS publisher to PUBLISH_TOPIC with a queue_size of 1
    pub = nh.advertise<sensor_msgs::PointCloud2>(PUBLISH_TOPIC, 1);
    // Spin
    ros::spin();
    // Success
    return 0;
}
```

List of Figures

List of Tables

List of Symbols

Variable	Description	SI unit
ω	angular speed	rad/s
V	linear speed	m/s

Acknowledgements

Lo sviluppo di questa tesi si pone come un traguardo per me, alla fine di un percorso iniziato ormai tre anni fa quando decisi d'intraprendere il passaggio da economia a ingegneria.

Desidero quindi ringraziare prima di tutto la mia famiglia, che da sempre mi supporta, credendo tanto quanto me in questo progetto. Senza il loro appoggio non sarei arrivato fino a qui. Una dedica in particolare va a mio nonno, per essere stato per me un esempio di dedizione al lavoro e forza di determinazione.

Ringrazio le persone che mi hanno accompagnato in questi anni e che tutt'ora mi sono vicine ogni giorno, con le quali ho condiviso momenti importanti che spero di ricordare a lungo.

Grazie ad Oversonic Robotics, a Fabio Puglia per avermi dato l'opportunità di lavorare a un progetto così ambizioso, all'ing. Lorenzo Romanini per il supporto e a tutte le persone incontrate a Besana che hanno alleggerito le giornate di lavoro.

Vorrei esprimere inoltre la mia gratitudine al professor Matteo Matteucci, per la sua pazienza e la sua disponibilità nell'affiancarmi in questa tesi.

Ringrazio il Politecnico di Milano e il professor Paolo Bolzern per avermi dato la possibilità d'intraprendere questo percorso, anche quando il mio background non lo consentiva. Ringrazio infine la città di Milano per avermi accolto e fatto crescere dal punto di vista umano e professionale in questi anni.